Materials and Methods

BASIC CELL CULTURE TECHNIQUES

Cell lines and culture conditions

The identities of all cell lines used in this study were confirmed using STR (short tandem repeat) profiling (University of Arizona Genetics Core). A2780 was grown in RPMI 1640 medium (Gibco, cat. no. 11875119) supplemented with 10% fetal bovine serum (FBS) (Sigma-Aldrich, cat. no. F4135), 2 mM glutamine (Lonza, cat. no. 17-605F), and 100 U/mL penicillin-streptomycin (Life Technologies, cat. no. 15140122). A2058, HCT116, HEK-293T, and PLAT-A cells were grown in DMEM (Gibco, cat. no. 11995073) supplemented with 10% FBS, 2 mM glutamine, and 100 U/mL penicillin-streptomycin. AGS was grown in F-12K (ATCC; cat. no. 30-2004) supplemented with 10% FBS, 2 mM glutamine, and 100 U/mL penicillin-streptomycin. HAP1 cells were grown in IMDM (Gibco, cat. no. 12440053) supplemented with 10% FBS, 2 mM glutamine, and 100 U/mL penicillin-streptomycin. MCF-10A was grown in DMEM/F-12 (Gibco, cat. no. 11320082), supplemented with 5% horse serum (Gibco, cat. no. 16050122), 20 ng/mL EGF (PeproTech, cat. no. AF-100-15), 0.5 ng/mL hydrocortisone (Sigma-Aldrich, cat. no. H0888), 100 ng/mL cholera toxin (Sigma-Aldrich, cat. no. C8052), 10 µg/mL insulin (Sigma-Aldrich, cat. no. I1882), 5 mM transferrin (Sigma-Aldrich, cat. no. T8158), and 100 U/mL penicillin-streptomycin. All cells were cultured in a humidified environment at 37˚C and 5% CO_2. Sources of the cell lines used in this manuscript are listed in Table S4.

Production of lentivirus and retrovirus

HEK293T (lentivirus) or PLAT-A (retrovirus) cells were transfected using the calcium-phosphate method (*68*). Virus-containing supernatant was harvested 48 to 72 hours post-transfection, filtered through a 0.45 µm syringe, and then frozen at -80˚C for later use or applied directly to cells with

4-10 µg/mL polybrene (Santa Cruz Biotechnology, Inc., cat no. SC-134220). The culture medium on target plates was changed 24 hours post-transduction.

PLASMID CLONING METHODS

CRISPR plasmid cloning

Guide RNAs for CRISPR experiments were designed with Benchling (www.benchling.com). Guides were cloned into the Lenti-Cas9-gRNA-GFP vector (Addgene #124770) or LRCherry2.1 (Addgene #108099) using a BsmBI digestion as previously described (*68*). Plasmids were transformed in Stbl3 E. coli (Thermo Fisher Scientific, cat. no. C737303) and sequence-verified to confirm the presence of the correct gRNA. CRISPR gRNA sequences are listed in Table S5A.

CRISPRi plasmid cloning

Guide RNAs for CRISPRi experiments were chosen from refs (*47*, *69*) and cloned into the LRG2.1 mCherry vector (Addgene #108099) as described above. Plasmids were transformed in Stbl3 *E. coli* and sequenced to confirm the presence of the correct gRNA sequence. CRISPRi gRNA sequences are listed in Table S5B.

Cloning of doxycycline-inducible plasmids

The *MDM4* coding sequence (NM_002393.5) was cloned into Lenti-X™ Tet-One™ Inducible Expression System (Takara Bio, cat. no. 631847). The resulting plasmid was then subject to whole-plasmid sequencing for verification. A2780 cells were transduced with pLVX-TetOne-MDM4-Puro and selected for with 1.5 µg/mL puromycin (InvivoGen, cat. no. ant-pr-1). Tight inducibility was confirmed through doxycycline (Sigma-Aldrich, cat. no. D3072) titration and quantitative real-time PCR. The final plasmid was deposited on Addgene (#195140). Similarly, coding sequences for *BCL9* (NM_004326.4), *MCL1* (NM_021960.5), *PFDN2* (NM_012394.4), *PPP1R15B* (NM_032833.5), and *PSMD4* (NM_002810.4) were cloned into the pLXV-TetOne

backbone and subject to sequence verification. Transduction and selection were performed as described above, and the final plasmids were deposited on Addgene (#202662-202666). Doxycycline-inducible plasmids are listed in Table S6.

KARYOTYPING AND DNA COPY NUMBER ANALYSIS

SMASH-Seq

Libraries for genomic copy number analysis were prepared as described in ref (*36*). In brief, genomic DNA was enzymatically fragmented to a mean size of ~40bp and ligated to generate long chimeric DNA molecules (~300-700bp) for sequencing. Fragment size selection and purification were done with Agencourt AMPure XP beads (Beckman Coulter, cat. no. A63881). Illumina-compatible NEBNext Multiplex Dual Index primer pairs and adapters (New England Biolabs, cat. no. E6440S) were added to each sample, and the products were pooled for next-generation sequencing (NGS). Libraries were sequenced using an Illumina MiSeq or NovoSeq sequencer. The generated reads were demultiplexed then mapped using a custom Nextflow (*70*) wrapper running *SMASH* built from MUMdex (*71*) (commit: 25e1f2f). Plots were generated via a custom script utilizing *tidyverse* (*72*) (v1.3.1) components run in the R programming environment (R Core Team 2022; v4.2.0).

G-banding karyotyping

A2780 samples were sent to Cell Line Genetics Inc. (www.clgenetics.com), and AGS and A2058 samples were sent to Karyologic Inc. (www.karyologic.com) for G-banding karyotyping. A minimum of 10 metaphase spreads per sample were counted and analyzed to prepare representative karyotype spreads.

TaqMan copy number analysis

Genomic DNA was extracted and isolated using the Qiagen DNeasy Blood & Tissue kit (Qiagen, cat. No. 69506). Reactions were prepared in quadruplicate, and target probes were duplexed with *RNaseP* (Applied Biosystems, cat. no. 4316831) or *TERT* (Applied Biosystems, cat. no. 4403316) as the reference assay. Quantitative PCR was performed using TaqPath ProAmp Master Mix (Applied Biosystems, cat. no. A30867) and quantified using the QuantStudio 6 Flex Real-Time PCR system (Applied Biosystems). Copy number analysis was performed as described in ref (*73*) and copy number calls were normalized to the near-diploid colorectal cancer cell line DLD1. To screen for chromosome arm loss, a minimum of three probes spanning the chromosome of interest were used, and the copy number calls for the individual probes were averaged to determine chromosome arm copy number. To screen for single copy gene deletions, two probes for the gene of interest were used, and the copy number calls for the individual probes were averaged to determine gene copy number. TaqMan copy number probes are listed in Table S7.

GENE EXPRESSION ANALYSIS

RNA-seq

Total cellular RNA was extracted using the Qiagen RNeasy Mini Kit (Qiagen, cat. no. 74106) and subjected to on-column DNase digestion (Qiagen, cat. no. 79254). Purified RNA samples were submitted to Novogene for RNA-seq and quantification. In brief, mRNA was purified from total cellular RNA using poly-T oligo-attached magnetic beads. After fragmentation, first strand cDNA was synthesized using random hexamer primers, followed by second strand cDNA synthesis. Subsequently, libraries were prepared with end repair, A-tailing, adapter ligation, size selection, amplification, and purification. Libraries were sequenced on an Illumina platform and paired-end reads were generated.

Raw data (raw reads) in fastq format were firstly processed through in-house Novogene Perl scripts to remove adapters, reads containing >10% undetermined bases, and low-quality reads

(≥50% of bases with Qscore ≤5). Reference genome and gene model annotation files were downloaded from genome website directly. An index of the reference genome was built using Hisat2 v2.0.5 and paired-end clean reads were aligned to the hg38 reference genome using Hisat2 v2.0.5. featureCounts v1.5.0-p3 was used to count the reads numbers mapped to each gene. The FPKM of each gene was calculated based on the length of the gene and reads count mapped to this gene. Read counts were normalized across samples via TMM normalization using edgeR v3.40.2 and grouping by ploidy (*74*). Gene Set Enrichment analysis was performed with the local version of the GSEA analysis tool http://www.broadinstitute.org/gsea/index.jsp, all Hallmark gene sets, and genes were ranked according to Signal2Noise. Following analysis by the GSEA analysis tool, select plots were reproduced using enrichplot v1.18.3 and clusterProfiler v4.6.2 in addition to tabulating enrichment values for all Hallmark gene sets (*75*, *76*).

Mass spectrometry

Proteomic analysis was conducted as previously described (*77*). In short, cell pellets were thawed and a VialTweeter device (Hielscher-Ultrasound Technology) was used to sonicate the samples (4 °C; 1 min; two cycles). The samples were centrifuged at 20,000 g for 1 hour to remove insoluble material. Protein concentration was measured using the Bio-Rad protein assay dye (Bio-Rad, cat. no. 5000006). 800 µg of protein per sample were diluted (final concentration = 2 µg/µL) using a 10 M urea/100 mM ammonium bicarbonate buffer, reduced by 10 mM DTT (1 hour; 56 °C), and alkylated by 20 mM IAA (1 hour; RT). The proteins were subjected to a precipitation-based digestion (*78*). Briefly, five volumes of precooled precipitation solution (50% acetone, 50% ethanol, and 0.1% acetic acid) were added to the samples. After overnight incubation at -20 °C, the samples were centrifuged (20,000 x g; 4 °C; 40 min). The precipitate was washed with precooled 100% acetone, centrifuged (20,000 x g; 4 °C; 40 min), and the remaining acetone was evaporated in a SpeedVac. For protein digestion, 300 µL of 100 mM NH4HCO3 with sequencing grade porcine trypsin (Promega) at a trypsin-to-protein ratio of 1: 20 were added and incubated

overnight at 37 °C. The resulting peptide samples were acidified with formic acid and desalted using a C18 column (MarocoSpin Columns, NEST Group INC.) according to the manufacturer's instructions.

1 µg of the peptide mixture was used for the LC-MS analysis as described previously (*77*, *79*). The LC separation was performed using an EASY-nLC 1200 system (Thermo Scientific) using a self-packed PicoFrit column (New Objective, Woburn, MA, USA; 75 µm × 50 cm length) with a ReproSil-Pur 120A C18-Q 1.9 µm resin (Dr. Maisch GmbH, Ammerbuch, Germany). A 120-min gradient length was used to elute peptides from the LC; with buffer B (80% acetonitrile containing 0.1% formic acid) from 5% to 37% and corresponding buffer A (0.1% formic acid in H2O). The flow rate was 300 nL/ min, and the temperature was controlled at 60 °C using a column oven (PRSO-V1, Sonation GmbH, Biberach, Germany). The Orbitrap Fusion Lumos Tribrid mass spectrometer (Thermo Scientific) coupled with a NanoFlex ion source (spray voltage of 2000 V, 275 °C) was used for the MS analysis. The method for DIA-MS consisted of a MS1 survey scan and 33 MS2 scans of variable windows (*80*, *81*). The MS1 scan parameters were set as follows: scan range 350–1650 m/z, resolution 120,000 at m/z 200, the AGC target 2.0E6, and the maximum injection time 100 ms. The normalized HCD collision energy was 28%. The MS2 scan parameters were the following: resolution 30,000 at m/z 200, the AGC target 1.5E6, and the maximum injection time 50 ms. The default peptide charge state was set to 2. Both of MS1 and MS2 spectra were recorded in a profile mode.

The DIA-MS data analysis was performed using Spectronaut v15 (*80*, *82*) using the library-free DirectDIA workflow (*80*, *83*) and the Swiss-Prot protein database (September 2020, 20,375 entries). The analysis was performed using default Spectronaut settings. Methionine oxidation and N-terminal acetylation were set as variable modifications, where carbamidomethylation at cysteine was set as a fixed modification. Both peptide- and protein-FDR were controlled at 1%,

and the resulting data matrix was filtered by “Qvalue”. The DIA quantification was performed using the MS2 level peak areas. Protein intensities were exported, log2-transformed and normalized using LOESS normalization prior to the subsequent analysis.

Quantitative real-time PCR

Total cellular RNA was extracted and isolated using the Qiagen RNeasy Mini Kit (Qiagen, cat. no. 74106). cDNA synthesis was performed using SuperScript IV VILO Master Mix (Invitrogen, cat. no. 11756500). Quantitative PCR was performed for the target genes using TaqMan Fast Advanced Master Mix (Applied Biosystems, cat. no. 4444963) and quantified using the QuantStudio 6 Flex Real-Time PCR system (Applied Biosystems). TaqMan gene expression assays are listed in Table S8 and qPCR primers are listed in Table S9.

Western Blotting

One day prior to lysate harvest, 500,000 cells were seeded in a six-well plate. Whole cell lysates were harvested and resuspended in RIPA buffer [25 mM Tris, pH 7.4, 150 mM NaCl, 1% Triton X 100, 0.5% sodium deoxycholate, 0.1% sodium dodecyl sulfate, protease inhibitor cocktail (Sigma, cat. no. 4693159001), and phosphatase inhibitor cocktail (Sigma, cat. no. 4906845001)]. Protein concentration was quantified using the RC DC Protein Assay (Bio-Rad; cat. no. 500–0119). Equal amounts of lysate were denatured and loaded onto a 10% SDS-PAGE gel. The Trans-Blot Turbo Transfer System (Bio-Rad) and polyvinylidene difluoride membranes were used for protein transfer. Antibody blocking was done with 5% milk in TBST (19 mM Tris base, NaCl 137 mM, KCl 2.7 mM and 0.1% Tween-20) for 1 hour at room temperature. The following antibodies and dilutions were used: p21 (Abcam; cat. no. ab109520) at a dilution of 1:1000 in 5% milk, p53 (Abcam; cat. no. ab1101) at a dilution of 1:1000 in 5% milk, p53 (Abcam; cat. no. ab32389) at a dilution of 1:1000 in 5% milk, phospho-p53 (Ser15) (Cell Signaling, cat. no. 9284S) at a dilution of 1:1000 in 5% milk, cleaved PARP (Asp214) (Cell Signaling; cat. no. 5625S) at a dilution of

1:1000 in 5% milk, and UCK2 (proteinTech; cat. no. 10511-1-AP) at a dilution of 1:1000 in 5% milk. Blots were incubated with the primary antibody overnight at 4°C. Anti-GAPDH (Santa-Cruz; cat. no. sc-365062) at a dilution of 1:20,000 in 5% milk, or anti-alpha tubulin (Sigma-Aldrich; cat. no. T6199) at a dilution of 1:20,000 in 5% milk was used as a loading control. Membranes were washed at room temperature three times (20 mins each) before they were incubated in secondary antibodies for an hour at room temperature. HRP goat anti-mouse (Bio-Rad; cat. no. 1706516) at 1:20,000 was used for tubulin, p53 (ab1101), MDM4, and GAPDH blots while HRP goat anti-rabbit (Abcam; cat. no. ab6721) at 1:20,000 was used for all other primary antibodies. Membranes were washed three times again (20 min each) and developed using ProtoGlow ECl (National Diagnostics; cat. no. CL-300) and autoradiographic film (Lab Scientific; XAR ALF 2025).

CHROMOSOME ENGINEERING

Chromosome elimination: ReDACT-NS

Generation of selection cassette: A centromere-proximal CRISPR gRNA was designed and cloned into the Lenti-Cas9-gRNA-GFP vector (Addgene #124770) for integration of the selection cassette. Homology arms for cassette integration were designated as the 180bp immediately upstream and downstream of the guide RNA targeting site. Adapters for PCR were added to the 3' end of the 180bp homology arms (Forward: gacattgattattgactagt; Reverse: ccatagagcccaccgcatcc), and the resulting 200bp ultramers were obtained from IDT. PCR for selection cassette production was performed with SeqAmp DNA Polymerase (Takara Bio, cat. no. 63850) using the ultramers as primers and AAT-PB-CD2APtk (Addgene #86004) or AAT-PB-PG2APtk (*84*) (Addgene #195124) as the template. The PCR products were purified and concentrated with the QIAquick PCR Purification kit (Qiagen, cat. no. 28106). Homology arm and ultramer sequences are listed in Table S9.

Knocking-in cassettes with CRISPR-mediated HDR: Cells were transfected with the PCR-purified selection cassette and integration gRNA CRISPR plasmid using Lipofectamine 3000 (Invitrogen, cat. no. L3000015) for A2780, AGS & HCT116 cells or FuGENE HD (Promega, cat. no. E2311) for A2058 cells. Integration of the cassette was selected with puromycin (InvivoGen, cat. no. ant-pr-1). Following selection, dsRed positive cells (when using Addgene #86004) or GFP positive cells (when using Addgene #195124) were single cell sorted onto 96-well plates, and clonal cell lines were established. Successful cassette integration was confirmed through PCR and sequencing. PCR check primer sequences are listed in Table S9. Integrant clones were subject to karyotypic validation through SMASH-Seq prior to inducing chromosome arm loss.

Inducing chromosome arm loss: A centromere targeting CRISPR gRNA was designed and cloned into the Lenti-Cas9-gRNA-GFP vector (Addgene #124770) for targeted chromosome elimination. Integrant clones were transfected with the centromere targeting gRNA CRISPR plasmid using Lipofectamine 3000 or FuGENE HD. Chromosome arm loss was selected for with 10 μM ganciclovir (Sigma Aldrich, cat. no. G2536). Following ganciclovir selection, dsRed or GFP negative cells were single cell sorted onto 96-well plates, and clonal cell lines were established. Clones were screened for targeted chromosome arm loss with TaqMan copy number assays as described below and chromosome elimination was confirmed through SMASH karyotyping. The aneuploidy-loss cell lines generated using this method are listed in Table S3.

Chromosome elimination: ReDACT-TR

Generation of the artificial telomere construct: The ReDACT-TR technique was motivated by the use of a telomere seed sequence to generate monosomic cells as described in ref (*1*). To enhance the efficacy of this approach, we created plasmids linking a telomere seed sequence with a puromycin selection marker, which allowed us to enrich for stably-transfected aneuploidy-loss cells using drug selection. These EF1a-Puro-Telo vectors (Addgene #195138 and #195139)

were generated by introducing a puromycin selection marker to a telomere seed sequence previously described in ref (*1*). This vector was digested with FastDigest KpnI (Thermo Fisher Scientific, cat. no. FD0524) and FastDigest BstZ17I (Thermo Fisher Scientific, cat. no. FD0704), and gel purified to obtain the artificial telomere construct.

Inducing chromosome arm-loss with CRISPR-mediated NHEJ: Cells were transfected with the purified artificial telomere construct and centromere-targeting gRNA CRISPR plasmids using Lipofectamine 3000 for AGS cells, or Fugene HD for MCF10A cells. Telomere replacement was selected for with puromycin, and puromycin resistant cells were single cell sorted onto 96-well plates. Clonal cell lines were established and screened for targeted chromosome arm loss with TaqMan copy number assays. Chromosome elimination was confirmed through SMASH karyotyping. The aneuploidy-loss cell lines generated using this method are listed in Table S3.

Chromosome elimination: ReDACT-CO

Cells were transfected with centromere targeting gRNA CRISPR plasmids using Lipofectamine 3000 or FuGENE HD. GFP+ cells were single cell sorted onto 96-well plates. Clonal cell lines were established and screened for targeted chromosome arm loss with TaqMan copy number assays. Chromosome elimination was confirmed through SMASH karyotyping. Chr1q_Centromere_Targeting_gRNA (Addgene #195125) and Chr1q_Cassette-Integration_gRNA (Addgene #195126) were used together to target chromosome 1q, Chr7_Centromere-Targeting_gRNA (Addgene #195129) was used to target chromosome 7p, and Chr8q_Centromere-Targeting_gRNA (Addgene #195128) was used to target chromosome 8q (Table S5A). The aneuploidy-loss cell lines generated using this method are listed in Table S3.

Choice of ReDACT techniques for each cell line

No underlying reasons motivated the selection of a specific ReDACT technique for each cell line. Our first approach, ReDACT-NS, was driven by the historical use of thymidine kinase for genomic modification in embryonic stem cells (*85*, *86*). However, after this project was initiated, several reports were published demonstrating accidental CRISPR-mediated chromosome loss without drug selection (*34*, *35*), which prompted us to experiment with the ReDACT-TR and ReDACT-CO techniques. Consequently, for most cell lines described in this manuscript, we initiated multiple ReDACT approaches at the same time, and then focused on characterizing the clones in which we were able to verify aneuploidy-loss first. Over time, we discovered that each technique had certain benefits and drawbacks. For instance, with ReDACT-NS, once a clone was isolated containing on-target integration of the *HSV-TK* cassette, it was relatively straightforward to produce a large number of aneuploidy-loss clones. In contrast, ReDACT-CO required only one round of single-cell cloning and was much faster than ReDACT-NS, but the overall efficiency of ReDACT-CO tended to be lower than ReDACT-NS. Importantly, we obtained consistent results on the effects of aneuploidy-loss regardless of the ReDACT technique that was ultimately used, underscoring our conclusion that aneuploidy-loss itself is the root cause of the observed phenotypes.

Generation of DLD1 trisomy 1 cells

The DLD1 trisomy 1 clone was generated as previously described in ref (*87*). In brief, DLD1 cells were transiently treated with 1 μM AZ3146 (Selleck Chemicals; cat. no. S2731) for 24 hours, and then the drug was washed out and the cells were allowed to recover for 24 hours. Following the recovery passage, single-cell sorting was performed to isolate individual aneuploid clones. SMASH-Seq was used to identify a clone harboring a trisomy of chromosome 1.

PHENOTYPIC CHARACTERIZATION OF ANEUPLOIDY-LOSS CELLS

Proliferation assays

Cells were seeded in 6-well plates at 100,000 cells per well. After 72 hours, cells were harvested, counted, and 100,000 cells were re-plated in fresh medium on 6-well plates. Cells were passaged ten times, and population doublings were calculated at each passage.

Soft agar assays

To assay colony formation in soft agar, a solution of 1.0% Difco Agar Noble (VWR Scientific, USA, cat. no. 90000–772) in sterile water was prepared. The 1% agar solution was mixed 1:1 with the base cell culture medium supplemented with 20% FBS, 4 mM glutamine, and 200 U/mL penicillin/streptomycin, or for MCF10A, supplemented with 10% horse serum, 40 ng/mL EGF, 1 ng/mL hydrocortisone, 200 ng/mL cholera toxin, 20 µg/mL insulin, 10 mM transferrin, and 200 U/mL penicillin streptomycin. 1 mL of this mixture was plated on each well of a 6-well plate and allowed to solidify at room temperature to form a base layer of 0.5% agar. Cells were then harvested and counted. For A2780 and A2058, 20,000 cells were seeded in 0.35% agar (1:1 mixture of 0.7% agar in sterile water and 2x supplemented growth medium). For AGS and MCF10A, 10,000 cells were seeded in 0.35% agar. For HCT116, 35,000 cells were seeded in 0.30% agar. Plates were left at room temperature to solidify and then placed in a humidified incubator at 37˚C and 5% CO_2. 1 mL of normal growth medium was added the next day, and every three days after. For soft agar assays involving doxycycline-inducible expression, cells were seeded in agar as described above, with the addition of 1 µg/mL doxycycline (Sigma-Aldrich, cat. no. D3072) to the base cell culture medium and to the normal growth medium replenished every three days. After 10-14 days, cells were fixed with 100% methanol, and stained with 0.01% crystal violet dissolved in 25% methanol. Colony formation was quantified by capturing z-stacks of several fields of view per well from at least three wells on a LSM 710 confocal microscope (Zeiss) or a Cytation5 imaging reader (BioTek Instrument, inc.), under either 4x, 5x, or 6x magnification. The average number of colonies was calculated by counting total number of colonies per field of view from multiple fields of view from at least three wells.

Xenograft assays

To assay tumor formation, cells were harvested and resuspended in cold PBS. For A2780 xenograft experiments, 3 million cells were injected in each flank of NU/J mice (Jackson Laboratory, cat. no. 002019). For A2058 xenograft experiments, 2 million cells were injected in each flank in NU/J mice. For HCT116 xenograft experiments, 4 million cells were injected in J:NU mice (Jackson Laboratory, cat. no. 007850). For MCF10A cells expressing $HRAS^{G12V}$, 10 million cells were injected in each flank in NU/J mice. For AGS xenograft experiments, the following conditions were tried: 5 million cells resuspended in PBS in each flank of NU/J mice (Jackson Laboratory, cat. no. 002019); 4 million cells resuspended in PBS in each flank of NGS mice (Jackson Laboratory, cat. no. 005557); and 15 million cells resuspended in a 1:1 PBS:Matrigel mixture in each flank of J:NU mice (Jackson Laboratory, cat. no. 007850). Cells were subcutaneously injected using a 1 mL 25G x 5/8 syringe (BD, cat. no. 309626). Mice were visually monitored for tumor formation routinely following injection. Once a tumor was visible, it was measured every three days by calipers. Tumor volume was calculated using the formula V = ½ (longer axis)(shorter axis). The mice were euthanized if their total tumor burden reached 2000 mm^3. The sample sizes for each mouse experiment are included in the "Sample Sizes and Statistical Techniques" section. In certain circumstances, mice were excluded from analysis for ethical reasons: some mice were euthanized before the end of the experiment and excluded from the tumor size calculations because their tumors ulcerated or grew too rapidly and compromised their wellbeing. In almost all cases in which a mouse was removed from the experiment and euthanized prematurely, it was due to the growth of the aneuploid cell line and not the aneuploidy-loss cell line. All mouse protocols were approved by the CSHL and Yale Institutional Animal Care and Use Committees.

Derivation and characterization of cell lines post-xenograft

To derive post-xenograft cell lines, the tumors were cut out using a sterilized pair of scissors. The tumors were placed into a chilled conical tube containing 2-3 mL of TrypLE Express Enzyme (Gibco; cat. no. 1260413) and transported on ice to a biosafety hood. The tumors were minced using sterilized scalpels and allowed to dissociate for 20-30 minutes in a 37˚C water bath. Cell culture medium was prepared using 2x the regular concentration of penicillin-streptomycin, and TrypLE was neutralized using an equivalent volume of this cell culture medium. The mixture was filtered through a cell strainer tube (Corning; cat. no. 352235) and plated onto a tissue culture treated 10 cm dish, with cell culture medium added to a total of 10 mL. The following day, upon cell adherence to the dish, the medium was replaced. When cells reached 70-80% confluence, they were frozen down in medium containing 2x the regular concentration of FBS and 10% DMSO. Cell pellets were simultaneously taken for downstream analyses, including TaqMan copy number assays and SMASH karyotyping. For subsequent phenotypic characterization, a fresh vial of cells was thawed and used in soft agar assays as described above.

KRAS genotyping

The sequence of *KRAS* exon 2 was obtained from GRCh38 using Benchling. Primers were designed to amplify the genomic region surrounding exon 2 (Table S9). PCR was performed with SeqAmp DNA Polymerase (Takara Bio; cat. no. 63850), and PCR products purified and concentrated with the QIAquick PCR Purification kit (Qiagen; cat. no. 28106). PCR products were sent for Sanger sequencing with both forward and reverse primers to Azenta Biosciences. The ratio of wild type to mutant base (G to A) to assess allelic ratio of $KRAS^{WT}$ to $KRAS^{G13D}$ was assessed using EditR (*88*).

Chromosome 1q SNP genotyping

Heterozygous SNPs on chromosome 1q were obtained from DepMap for A2058 and AGS, and the sequences around these loci were obtained from GRCh38 using Benchling. Primers were

designed to amplify the genomic region surrounding these SNPs in *OLFML2B* and *PPFIA4* in A2058, and *ASH1L* and *LGR6* in AGS respectively (Table S9). PCR was performed with SeqAmp DNA Polymerase, and the PCR products were purified and concentrated with the QIAquick PCR Purification kit. PCR products were sent for Sanger sequencing with both forward and reverse primers to Azenta Biosciences. We validated that these SNPs were heterozygous in the parental 1q trisomy lines and we discovered that these SNPs had underwent LOH in the 1q disomy lines. In samples with chromosome 1q regain, sequencing was performed at these loci to differentiate between endogenous and exogenous regain. The regain event was determined to be endogenous if the loss of heterozygosity was maintained, whereas exogenous regain events were marked by the re-emergence of heterozygosity. Two representative genes, *OLFML2B* in A2058, and *ASH1L* in AGS, are shown in Figure S13.

Cell cycle analysis

One day prior to cell cycle analysis, 1.5-2 million cells were plated onto a 10 cm dish. Cells were harvested by trypsinization with TrypLE, followed by centrifugation at 1,000 rpm for 5 minutes, aspiration of the media, and resuspension of the cell pellet in 1 mL PBS. Cells were added dropwise to 4mL of ice cold 100% ethanol and fixed at -20˚C for 5-15 minutes. Fixed cells were pelleted by centrifugation at 1,000 rpm for 5 minutes, resuspended in PBS containing 0.05% Triton X-100, 10 µg/mL RNAse A (Invitrogen, cat no. A32078), and 20 µg/mL propidium iodide (Life Technologies, cat. no. P3566), filtered through a cell strainer FACS tube cap. Cells were incubated for 30 minutes at room temperature in the dark. Cell cycle analysis was measured by flow cytometry (Miltenyi Biotech).

Senescence assay

Senescence-associated β-galactosidase staining was performed using a senescence β-galactosidase staining kit (Cell Signaling Technology, cat. no. 9860) according to the

manufacturer's instructions. Briefly, in a 6-well plate, the medium was discarded, and the cells were rinsed once in PBS. The cells were then fixed in a fixative reagent for 15 minutes at room temperature. The cells were then rinsed twice in PBS and incubated overnight at 37˚C without CO_2 in the β-galactosidase staining solution. The cells were imaged and analyzed under a light microscope (20X magnification, Olympus CKX53).

Nomination of candidate genes on chromosome 1q

A set of 16 genes encoded on chromosome 1q that could potentially contribute to the "1q aneuploidy addiction" phenotype was selected based on three primary criteria. First, we reasoned that dosage-sensitive drivers of chromosome 1q gains may sometimes also drive selection for focal or sub-chromosomal amplifications. We therefore selected genes that were located in or near segments of chromosome 1q that are recurrently subject to focal or sub-chromosomal amplification, as reported in ref. (*89*). Second, we reasoned that candidate driver genes should cause a loss in cell fitness when the expression of that gene is ablated, and so we only considered genes that had negative gene effect scores in CRISPR screens reported on DepMap (*90*). Third, we conducted literature searches on candidate genes, and we prioritized for cellular testing genes that had previously been associated with tumorigenesis. These analyses led us to produce a list of 16 candidate genes encoded on chromosome 1q (Table S5A). In parallel, our analysis of gene expression and mutual exclusivity associated with chromosome 1q indicated that the p53 pathway was affected by 1q-loss, causing us to first focus on *MDM4* as a candidate 1q driver.

CRISPRi competition assays

CRISPRi competition assays for candidate 1q driver genes were performed as described in ref (*48*). In brief, A2780 cells were transduced with a dCas9-KRAB construct (Addgene #85969).

dCas9-KRAB expressing TagBFP+ cells were purified using flow cytometry. For competition assays, dCas9-KRAB expressing cells were transduced with guides in vectors co-expressing mCherry that targeted the candidate genes. Three days post-transduction, cells were subject to flow cytometry analysis (Miltenyi Biotech) to assess the starting percentage of mCherry+ cells. Cells were re-plated, and timepoints were taken every three days through the conclusion of the assay at the fifth timepoint. To normalize for differences in starting percentages of mCherry+ cells, fold change, defined as (starting % positive)/(% positive at timepoint), was calculated at each timepoint. CRISPRi gRNA sequences are listed in Table S5B.

Assessing cellular sensitivity to UCK2 poisons and other anti-cancer agents

A 72-hour drug assay was performed to assess cellular sensitivity to different anti-cancer compounds. One day prior to the addition of the drug, 25,000 cells were plated into individual wells of a 6-well plate. The following day, upon cell adherence to the plate, the medium was discarded and replaced with drug-containing medium at varying concentrations. The cells were grown in the presence of the drug for 72 hours. Following this, the cells were harvested and counted. The following drugs were tested: RX-3117 (MedChemExpress; cat. no. HY-15228), 3-deazauridine (Cayman Chemical; cat. no. 23125), doxorubicin (Selleck Chemicals; cat. no. S1208), gemcitabine (Selleck Chemicals; cat. no. S1714), olaparib (Selleck Chemicals; cat. no. S1060), and CGS-15943 (Tocris; cat. no. 1699).

OTHER GENETIC MANIPULATIONS

Generation of control clones

Rosa26 gRNA clones: A CRISPR guide was designed to target the noncoding *Rosa26* locus and cloned into the Lenti-Cas9-gRNA-GFP vector (Addgene #124770) as described above. Cells were transfected with the *Rosa26* targeting gRNA CRISPR plasmid using Lipofectamine 3000,

and GFP+ cells were single cell sorted onto 96-well plates. Clonal cell lines were established and subject to karyotypic validation through SMASH karyotyping prior to phenotypic characterization.

1q, 7p, and 8q gRNA clones: Cells were transfected with centromere-targeting gRNA CRISPR plasmids using Lipofectamine 3000 and clonal cell lines were established as described above for ReDACT-CO (Table S5A). Clones that maintained an extra copy of the targeted chromosome, as revealed by TaqMan copy number assays and SMASH-Seq, were used as control clones.

Olfactory gene deletions: CRISPR guides were designed to flank the coding sequence of the targeted olfactory gene and cloned into the Lenti-Cas9-gRNA-GFP vector (Addgene #124770) as described above. Cells were transfected with the olfactory gene deletion guides using Lipofectamine 3000, and single GFP+ cells were sorted onto 96-well plates. Clonal cell lines were established and screened for single copy deletions of the targeted olfactory genes with TaqMan copy number assays as described above. To exclude the possibility of a chromosome truncation event, additional TaqMan copy number assays were performed with probes telomeric to the targeted gene. Clones with single copy deletions of the targeted olfactory gene were subject to karyotypic validation through SMASH-Seq prior to phenotypic characterization.

Generation of Cassette Deletion Clones: A2780 and AGS integrant clones were co-transfected with a centromere targeting gRNA and a cassette proximal gRNA using Lipofectamine 3000. Cassette deletion was selected for with 10 μM ganciclovir (Sigma Aldrich, cat. no. G2536). Following ganciclovir selection, dsRed or GFP negative cells were single cell sorted onto 96-well plates, and clonal cell lines were established. Clones were screened for cassette loss with PCR primers spanning the deletion region (Table S9) and cassette deletion independent of any other karyotypic alterations was confirmed through SMASH karyotyping.

Deletion of a single copy of *MDM4* or *UCK2*

CRISPR guides were designed to flank the coding sequence of the targeted gene and cloned into the Lenti-Cas9-gRNA-GFP vector (Addgene #124770) as described above. For dual guide plasmids, dual guide gene blocks were ordered from IDT and cloned into the Lenti-Cas9-gRNA-GFP vector using NEBuilder HiFi DNA Assembly (New England Biolabs, cat. no. E2621L). CRISPR gRNA sequences are listed in Table S5A. Cells were transfected with the gene deletion guides using Lipofectamine 3000, and GFP+ cells were single cell sorted onto 96-well plates. Clonal cell lines were established and screened for single copy deletions of targeted genes with TaqMan copy number assays as described above. To exclude the possibility of a chromosome truncation event, additional TaqMan copy number assays were performed with probes telomeric to the targeted gene. Clones with single copy deletions of the targeted genes were subject to karyotypic validation through SMASH karyotyping prior to phenotypic characterization.

Transformation of MCF10A with *HRAS*^{G12V}

pBABE-HRASV12-Hyg (Addgene #195143) was generated by cloning *hRASV12* from pBABE-HRASV12-puro (Addgene #9051) into pBABE-hyg (Addgene #1765) by digestion of both plasmids with BamHI and SalI, gel purification of digested DNA, ligation, and transformation into Stbl3 E. coli. The plasmid sequence was verified by sequencing. Viral preparation and transduction were performed as described above.

Derivation of *TP53*-knockout clones

TP53-targeting gRNAs were designed and cloned into the Lenti-Cas9-gRNA-GFP vector (Addgene #124770) for generating *TP53-KO* clones. In parallel, an *AAVS1*-targeting gRNA was utilized to generate isogenic *TP53*-WT control clones. A2780 cells were transfected with these CRISPR gRNA plasmids and GFP+ cells were single cell sorted onto 96-well plates. Clonal cell

lines were established and screened for *TP53-KO* through western blotting. Clones were subject to karyotypic validation through SMASH karyotyping prior to phenotypic characterization.

Generation of HAP1 *UCK2-KO* cells

HAP1 cells harboring a CRISPR-induced frameshift mutation in the *UCK2* gene were purchased from Horizon Discovery (cat. no. HZGHC007067c006). Loss of UCK2 expression was verified by western blotting.

Generation of A2780 cells constitutively overexpressing chromosome 1q genes

A2780 cells were transduced with pLV-Bsd-CMV-hUCK (Addgene #195141), pLV-Bsd-CMV-MDM4 (Addgene #202669), pLV-Neo-CMV-MCL1 (Addgene #202668), or pLV-Hyg-CMV-BCL9 (Addgene #202667) and selected with 4 µg/mL blasticidin (InvivoGen; cat. no. ant-bl-1), 200 µg/ml G418 (InvivoGen: cat. no. ant-gn-1), or 100 µg/ml hygromycin (InvivoGen: cat. no. ant-hg-1). The plasmid sequences were verified by sequencing. Viral preparation and transduction were performed as described above. Constitutive overexpression plasmids are listed in Table S6.

SAMPLE SIZES AND STATISTICAL TECHNIQUES

For all soft agar experiments, the data displayed represent colony counts from at least 15 independent fields of view. All soft agar experiments were conducted at least twice (two or more independent biological replicates), and representative experiments are shown. Boxplots for soft agar assays display the 25th, 50th, and 75th percentiles of colonies per field, and the whiskers display the 10th and 90th percentiles.

For all drug sensitivity experiments, cells were plated in duplicate or triplicate and counted twice. All drug sensitivity experiments were performed at least three times (three or more independent

biological replicates), with the exception of the control experiments in Figure S19D, which were performed once. Bar graphs in drug sensitivity assays display the means ± SEM.

For the proliferation experiments in Figure S6A, S6B, S6C, and S6E, two independent biological replicates were performed, and the average of both replicates are displayed. The proliferation experiment in Figure S6D was performed once.

For the competition experiment in Figure 6E-F, two independent experiments were performed: one when cells were mixed at an 80-20 ratio and one when cells were mixed at a 90:10 ratio. Similar results were obtained in both experiments.

The number of mice used in each xenograft experiment are as follows: 2E: n = 10 mice for A2058 xenografts; n = 5 mice for A2780 1q-loss c1 xenografts; n = 6 mice for A2780 1q-loss c2 xenografts. 2H: n = 10 mice for 1q-loss c2 xenografts; n = 9 mice for 1q-loss c3 xenografts. 3D: n = 8 mice for 7p-loss c1 xenografts; n = 15 mice for 7p-loss c2 and 8q-loss c1 xenografts; n = 9 mice for 8q-loss c2 xenografts. 3H: n = 9 mice for each experiment. 4A: n = 8 mice. 4D: n = 9 mice. 4E: n = 10 mice. 4G: n = 9 mice. S5A: n = 10 mice. S5B: n = 10 mice. S5C: n = 10 mice. S11A: n = 7 mice. Tumor growth curves in xenograft assays display the means ± SEM.

Data were analyzed by unpaired t-tests in the following figures: 2D, 2G, 3C, 3G, 4H, 5G, 5H, 5M, 5N, 6B, 6C, 6D, S6A, S6B, S6C, S6D, S6E, S13D-E, S14E, S15A, S15B, S16D, S17C-E, S18A, S18C-E, S18G, S20E, and S21D-E. Data were analyzed by chi-square tests in Figure 4F. Data were analyzed by Fisher's exact test in Figure S18F.

The raw data from each experimentally-generated figure are included in Table S10.

COMPUTATIONAL APPROACHES

Copy number timing analysis

Raw whole genome sequencing (WGS) data in Bam or Fastq formats were downloaded from public databases provided by the original publications (*21*, *22*, *91*). We used ith.Variant pipeline (https://github.com/SunPathLab/ith.Variant) to call somatic copy number alterations (SCNA) and point mutations and to determine the clonality of these somatic variants (*92*). In total, 38 breast cancer samples (BRCA) from 21 patients and 37 melanoma (MEL) primary tumor samples (all paired with normal control samples) passed our WGS data quality control and were included in the analysis. To reconstruct the evolutionary history of SCNAs in patient tumors, we applied BUTTE to infer the initiation time of clonal CN gains. We define the initiation time as the time fraction when the first gain occurs for a clonal SCNA. In brief, BUTTE estimates the initiation time of complex gains (or gains involving multiple steps) by modeling the quantitative relationship between point mutations and paths of copy number events. To do so, it first adopts the expectation–maximization (EM) algorithm to find the allele state distribution of point mutations. BUTTE then either directly solves the timing for SCNAs with identifiable CN history matrices (*93*) or adopts linear programming to calculate the upper bounds of the initiation time if the underlying linear system is underdetermined (multiple history matrices exist for an SCNA)(*20*). We identified clustered gains by clustering the inferred timing via nonparametric density estimation (*94*). Genome doubling was identified as the cluster containing more than 40% of the segments. The accession numbers for the datasets are as follows: JGAD000095, EGAD00001002696, and EGAD00001003388.

Detecting recurrent early gains

To identify genomic regions exhibiting recurrent early gains across patients, we scanned hg38 genome with bins of 1 million bp in size and ranked the bins in each sample according to the timing of the respective initiating gain. The timing values were jittered to avoid ties. We then

subtracted from each bin the middle rank of the respective sample. The middle rank was the expectation value of the ranks under the assumption that the null hypothesis holds: no regions show recurrent early gain across patients. For each tumor type, we summed the resulting ranks across patients for each bin. Division of the rank sums by its standard deviation yielded normalized rank sums which approximately follow a standard normal distribution if the null hypothesis is fulfilled. A large negative normalized rank sum would reject the null hypothesis and indicate recurrent early initiating gains. To evaluate the frequency of gains for each genomic bin across patients, we ranked the segment mean (read depth ratio between the tumor and normal samples) as we did for the timing values, and then performed the same rank sum normalization. A large positive normalized rank sum for the segment mean would suggest frequent gains across patients.

Analysis of mutual exclusivity between aneuploidy and oncogenic mutations

To analyze the mutual exclusivity between aneuploidy and oncogenic mutation, we started from the MSK-MET (*26*) dataset available via the public cBioPortal datahub. In order for a given chromosomal arm and oncogene to be compared, we required that the data pass a set of quality filters. We required all cancer types to have ≥ 25 patients and selected a representative sample for each patient based on available mutation and arm gain data. We built sets of genes and arms by cancer type by applying additional requirements by cancer. The sets of genes we analyzed started from the IMPACT-505 geneset and we required each gene be mutated in ≥ 2% of patients by cancer type. The sets of arms we analyzed started from all previously generated arm gain data by sample and each arm was required to exceed a minimum of 100 patients or ≥ 2% of patients experiencing arm gain by cancer type. Once we had our cleaned sets of genes and arms by cancer, we calculated contingency tables for each combination and conducted a two-sided Fisher's exact test to compute p-values and odds ratios for each gene X arm combination. We converted these p-values into Z scores for further comparisons and applied the sign of the

negative log2 of the odds ratio to represent the direction of the relationship; therefore, a large positive Z would suggest significant mutual exclusivity, while a large negative Z would suggest significant co-occurrence. We repeated this process in a pancancer analysis by utilizing the same cleaned data and pooling all patients, genes, and arms into a single cohort. All mutual exclusivity analysis was automated using Nextflow (*70*) and Conda (*95*), starting from downloading MSK-MET data through to generation of Figures 1D-E and S1 and Table S1.

Analysis of copy number alterations and patient survival

To examine the relationship between copy number gains, mutations, and cancer patient outcomes in TCGA, univariate Cox proportional hazards models were used as described in refs (*96*, *97*). In brief, TCGA copy number data (broad.mit.edu_PANCAN_Genome_Wide_SNP_6_whitelisted.seg, available at https://gdc.cancer.gov/about-data/publications/pancanatlas) and TCGA mutation data (mc3.v0.2.8.PUBLIC.maf.gz, available at https://gdc.cancer.gov/about-data/publications/pancanatlas) were combined with patient outcomes data described in ref (*98*). Selection of the clinical endpoint for each cancer type was based on the recommendations provided by ref (*98*) based on data quality, cohort size, and the number of events that were observed. TCGA copy number data was generated as relative copy number values for particular chromosomal intervals. This data was translated to produce a single copy number value on a per-gene basis, based on the observed copy number at each gene's transcription start site. This annotation was performed using mapping data from GENCODE v32. Z scores for copy number changes and for mutations in common cancer driver genes were calculated using Cox proportional hazards regression. For the copy number analysis presented in Figure S2, genes were mapped back to chromosome bands, and the top-scoring gene (based on the pan-cancer Stouffer's Z score) was identified for each band. For the mutation analysis presented in Figure S2, a gene was considered to be mutated if there was a single non-synonymous mutation at any

codon within the gene. Non-synonymous mutations included: missense, nonsense, frameshift deletion, splice site, frameshift insertion, inframe deletion, translation start site, nonstop mutation, and in-frame insertion. Additional clinical data presented in Figure S2E were downloaded from cBioportal.

Analysis of aneuploidy-associated gene expression

Chromosome copy number data for cancers from TCGA were downloaded from ref (*1*). Chromosome copy number data for the Cancer Cell Line Encyclopedia was downloaded from ref (*65*). Gene expression data for cancers from TCGA was downloaded from the TCGA PanCanAtlas (EBPlusPlusAdjustPANCAN_ IlluminaHiSeq_RNASeqV2.geneExp.tsv, available at https://gdc.cancer.gov/about-data/publications/ pancanatlas). Gene expression data for the Cancer Cell Line Encyclopedia was downloaded from DepMap (www.depmap.org).

DATA VISUALIZATION

Scientific illustrations were generated with Biorender. Most graphs were generated using GraphPad Prism. Boxplots display the 25th, 50th, and 75th percentiles of colonies per field, while the whiskers represent the 10th and 90th percentiles. Unless otherwise indicated, bar graphs and XY plots display the means ± SEM.

Supplementary Text. Considering alternate explanations for the loss of fitness in engineered 1q-disomic cancer cells

In order to generate isogenic cancer cells that have or lack specific aneuploid chromosomes, we developed and applied a suite of CRISPR tools for chromosome engineering called ReDACT. We discovered that eliminating the trisomy of chromosome 1q severely compromised malignant potential in multiple independent cancer cell lines. We considered and rigorously evaluated the possibility that the loss of fitness observed among the 1q-disomic clones could be a consequence of our chromosome engineering methodologies, rather than the subsequent change in cellular karyotype. However, multiple lines of evidence indicate that this loss of fitness is best explained as a specific outcome of eliminating trisomy-1q and not a consequence of our experimental approach:

1) We constructed and tested control clones that mimicked the methods used to produce 1q-loss events (Fig. S7). These control manipulations included treating cells with ganciclovir to select for TK-loss, using CRISPR to induce terminal chromosomal truncations, and using CRISPR to delete olfactory receptor genes (Fig. S8A). In total, we generated 37 control clones, and we found that every single control clone exhibited superior anchorage-independent growth compared to the 1q-disomic clones (Fig. S8B-E).
2) We used the same ReDACT pipeline to eliminate the trisomy of chromosome 7p in A2058 cells and the trisomy of chromosome 8q in A2058 and HCT116 cells. If the loss of fitness observed in our 1q-disomic clones was a non-specific consequence of our chromosome engineering techniques, then we would expect to see similar phenotypes across different aneuploidy-loss clones. However, we consistently observed that eliminating the trisomy of chromosome 1q produced a more-severe fitness defect than eliminating the trisomy of chromosome 7p or 8q (Fig. 3).

3) If an off-target effect of CRISPR was the cause of the reduced fitness upon 1q-loss, then we would not expect to see any selective pressure to restore the 1q trisomy. However, upon prolonged growth of the 1q-disomic clones in vitro or in vivo, we observed that many cell populations spontaneously recover an extra copy of chromosome 1q, and these 1q-restored cells exhibit improved colony-formation ability relative to the 1q-disomic clones (Fig. 4A-F).

We believe that the results described above are most consistent with a model in which 1q-aneuploidy promotes cancer growth.

In this manuscript, we demonstrated that eliminating the trisomy of chromosome 1q consistently decreased the expression of genes that were encoded on chromosome 1q, and the effects of 1q trisomy could be partially phenocopied by manipulating the expression levels of 1q genes like *MDM4*. However, we recognize that engineering the loss of a copy of chromosome 1q both decreases the dosage of chromosome 1q genes and also eliminates any unique mutations that were encoded on that homolog. Correspondingly, we considered the possibility that the effects of 1q-loss could be mediated in part by eliminating unique driver mutations that these cell lines had acquired on chromosome 1q. To explore this possibility, we evaluated all non-synonymous mutations on chromosome 1q in the 1q-trisomic cancer cell lines used in this study. Using data acquired from DepMap, we found 25 1q mutations in A2780, 19 1q mutations in A2058, and 52 1q mutations in AGS. We cross-referenced these mutations with the Catalogue of Somatic Mutations in Cancer (COSMIC) database to examine if any mutations were recurrently observed or causally implicated in human cancers. None of the 96 mutations present on chromosome 1q in A2780, A2058, and AGS were identified as mutational hotspots in the COSMIC database, and none of the genes affected by mutations were included in the Cancer Gene Census. Next, we investigated the list of cancer driver genes identified by Vogelstein et al. (*99*), and we found that

none of the 1q genes affected by mutations in these cell lines were annotated as likely drivers. Lastly, we examined MSK-IMPACT, a panel of 505 genes associated with both common and rare cancers (*100*). None of the 1q mutated genes are included in this panel. For these reasons, we believe that the mutations found on chromosome 1q in these cell lines likely represent passenger events, rather than cancer drivers. Nonetheless, we do not rule out the possibility that the loss of specific point mutations could influence the effects of aneuploidy-elimination in other experiments. For instance, as described in Figure 4G, we speculate that the effects of gaining chromosome 12 in HCT116 is mediated in part by the acquisition of an extra copy of the mutant $KRAS^{G13D}$ allele, and loss of a chromosome containing mutant *KRAS* may have different consequences than loss of a chromosome containing wild-type *KRAS*.

Supplementary Figure 1

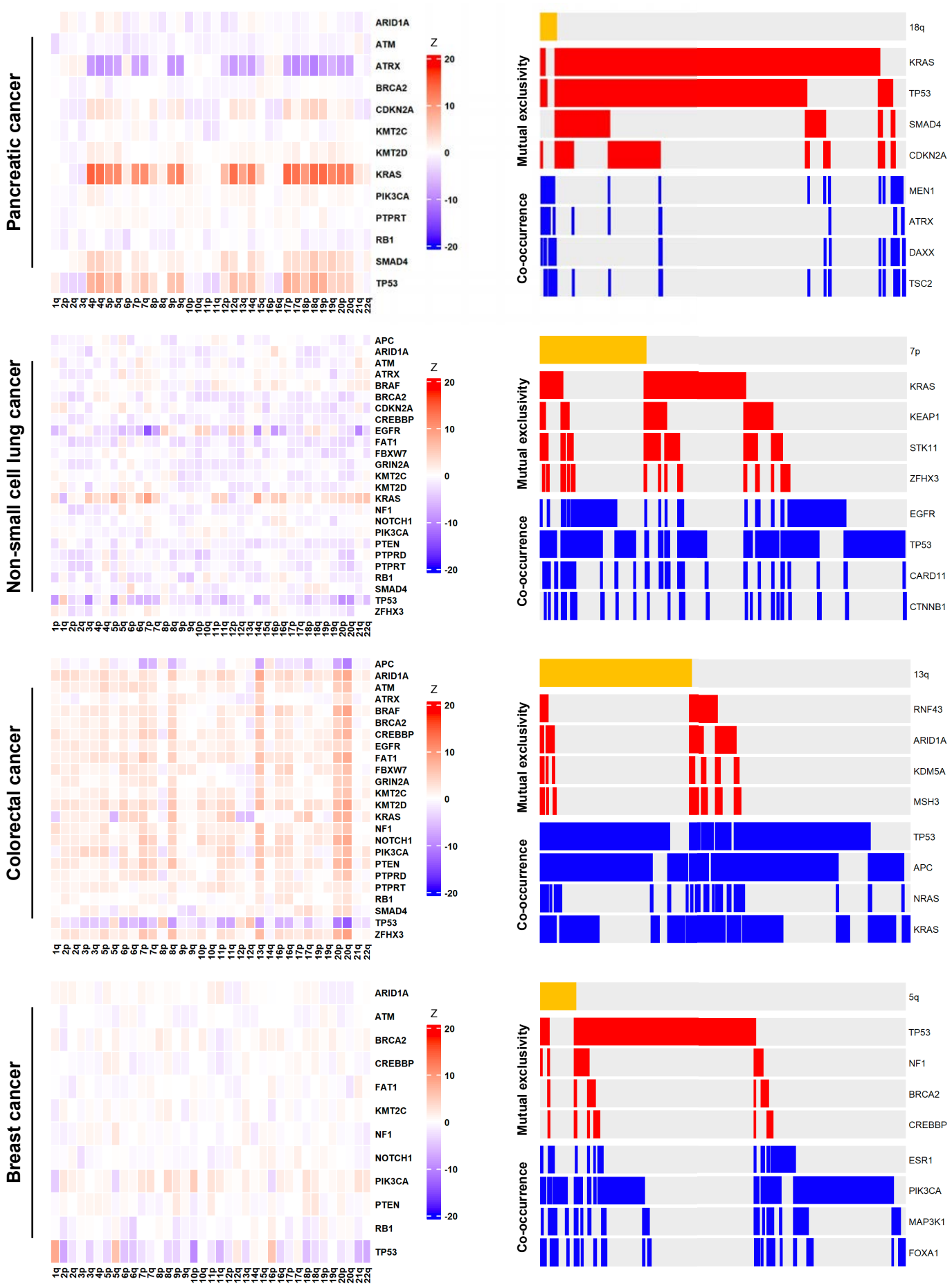

Figure S1. Mutual exclusivity between chromosome arm gains and mutations in cancer driver genes in individual cancer types.

(Left) Heatmaps are displayed demonstrating mutual exclusivity (in red) and co-occurrence patterns (in blue) between chromosome arm gains and mutations in common cancer driver genes within four individual cancer types: pancreatic cancer, non-small cell lung cancer, colorectal cancer, and breast cancer.

(Right) Oncoprint panels highlighting mutual exclusivity and co-occurrence patterns within individual cancer types for specific chromosome gain events. The complete results of this analysis are included in Table S1.

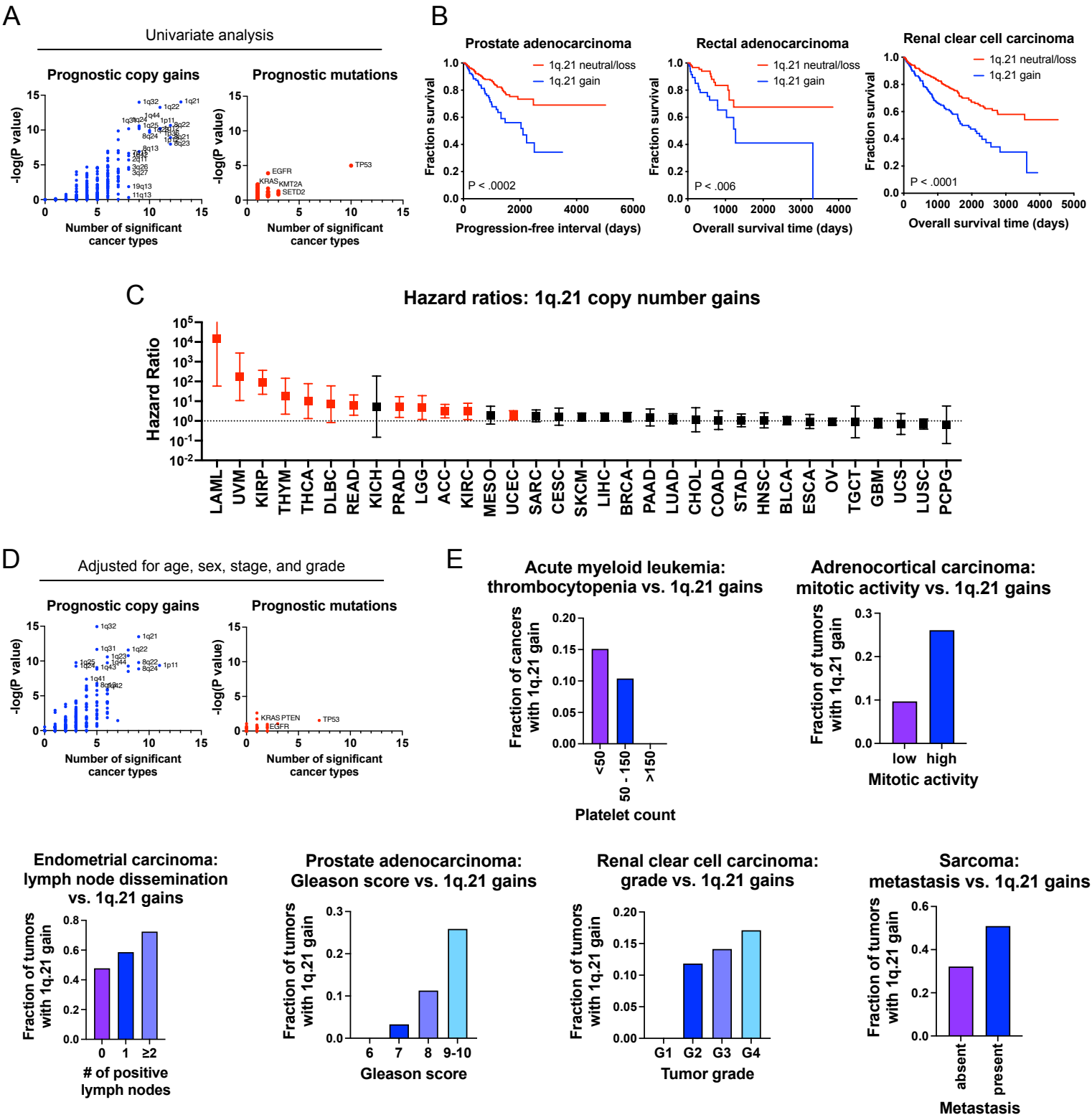
A
Univariate analysis
Prognostic copy gains
Prognostic mutations
-log(P value)
Number of significant cancer types
EGFR
KRAS
KMT2A
SETD2
TP53
B
Prostate adenocarcinoma
Rectal adenocarcinoma
Renal clear cell carcinoma
1q.21 neutral/loss
1q.21 gain
Fraction survival
P < .0002
P < .006
P < .0001
Progression-free interval (days)
Overall survival time (days)
C
Hazard ratios: 1q.21 copy number gains
Hazard Ratio
LAML UVM KIRP THYM THCA DLBC READ KICH PRAD LGG ACC KIRC MESO UCEC SARC CESC SKCM LIHC BRCA PAAD LUAD CHOL COAD STAD HNSC BLCA ESCA OV TGCT GBM UCS LUSC PCPG
D
Adjusted for age, sex, stage, and grade
Prognostic copy gains
Prognostic mutations
-log(P value)
Number of significant cancer types
KRAS PTEN EGFR
TP53
E
Acute myeloid leukemia: thrombocytopenia vs. 1q.21 gains
Fraction of cancers with 1q.21 gain
<50
50 - 150
>150
Platelet count
Adrenocortical carcinoma: mitotic activity vs. 1q.21 gains
Fraction of tumors with 1q.21 gain
low high
Mitotic activity
Endometrial carcinoma: lymph node dissemination vs. 1q.21 gains
Fraction of tumors with 1q.21 gain
0 1 ≥2
# of positive lymph nodes
Prostate adenocarcinoma: Gleason score vs. 1q.21 gains
Fraction of tumors with 1q.21 gain
6 7 8 9-10
Gleason score
Renal clear cell carcinoma: grade vs. 1q.21 gains
Fraction of tumors with 1q.21 gain
G1 G2 G3 G4
Tumor grade
Sarcoma: metastasis vs. 1q.21 gains
Fraction of tumors with 1q.21 gain
absent present
Metastasis

Figure S2. Specific copy number gains, particularly involving chromosome 1q.21, are associated with disease progression and patient death.

(A) A scatterplot displaying the relationship between copy number gains for each chromosome band (left) and mutations (right) and patients' outcomes across 32 cancer types from TCGA (*97*). Significance was determined by calculating univariate Cox proportional hazards regression models for each data type. The complete results for this analysis are presented in Table S2A.

(B) Kaplan-Meier plots displaying the relationship between 1q.21 copy number gains and disease progression in prostate adenocarcinoma, rectal adenocarcinoma, and renal clear cell carcinoma.

(C) A forest plot showing hazard ratios and 95% confidence intervals for Cox proportional hazards regression between 1q.21 copy number and patient outcome for each of the indicated cancer types. The hazard ratios plotted in red represent those that are significant at a $p < 0.05$ threshold.

(D) A scatterplot displaying the relationship between copy number gains for each chromosome band (left) and mutations (right) and patients' outcomes across 32 cancer types from TCGA (*97*). Significance was determined by calculating multivariate Cox proportional hazards regression models for each data type, adjusting each model for patient age, sex, tumor stage, and tumor grade. The complete results for this analysis are presented in Table S2B.

(E) Chromosome 1q.21 gains are associated with hallmarks of disease progression risk in various cancer types.

Supplementary Figure 3

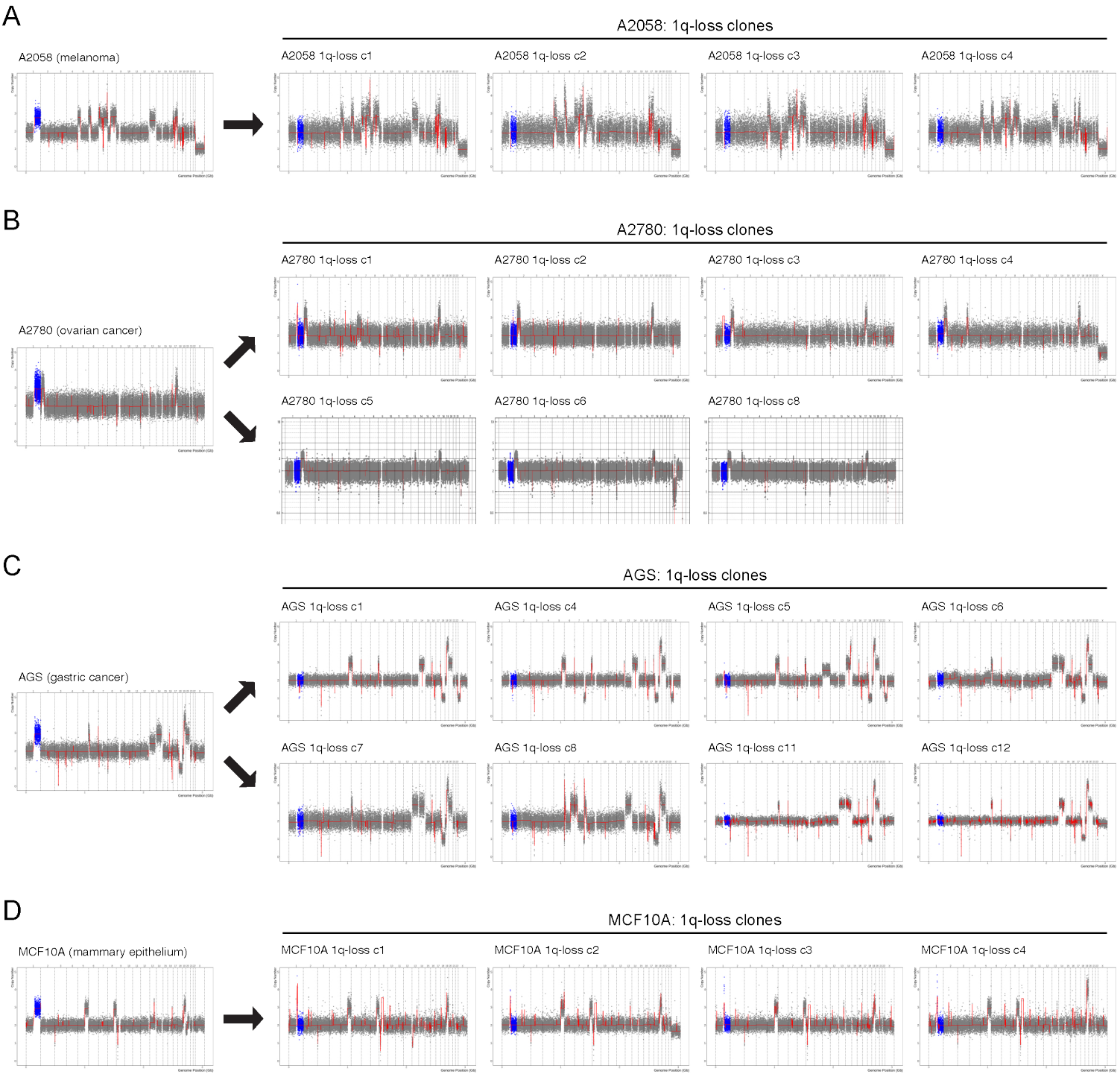

Figure S3. Additional karyotypes of 1q-disomic clones.

(A) SMASH karyotypes of 1q-disomic clones generated from the 1q-trisomic cancer cell line A2058.

(B) SMASH karyotypes of 1q-disomic clones generated from the 1q-trisomic cancer cell line A2780.

(C) SMASH karyotypes of 1q-disomic clones generated from the 1q-trisomic cancer cell line AGS.

(D) SMASH karyotypes of 1q-disomic clones generated from the 1q-trisomic immortalized mammary epithelial cell line MCF10A.

For all karyotypes in A-D, chromosome 1q is highlighted in blue. A complete list of aneuploidy-loss clones is included in Table S3.

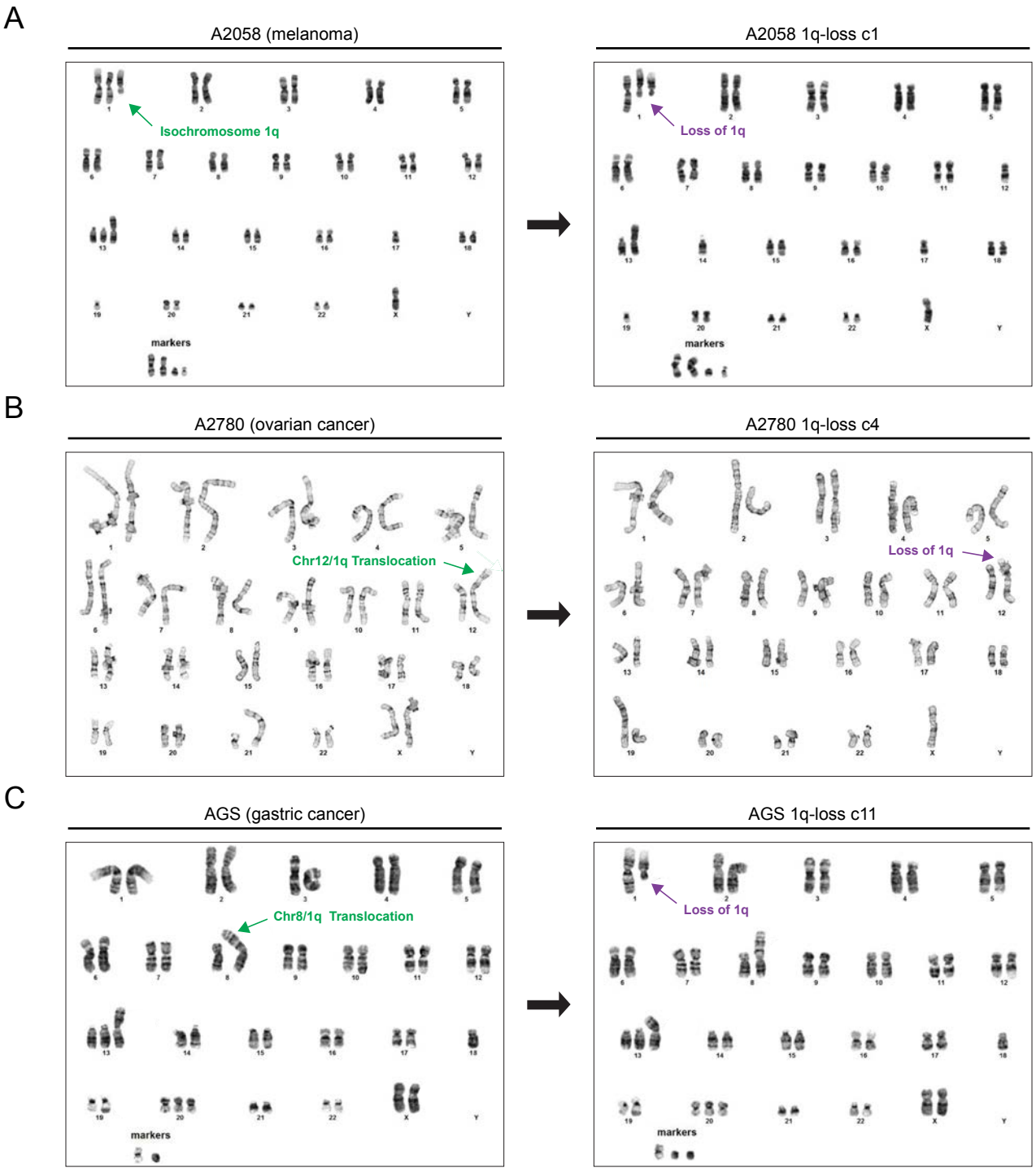
A
A2058 (melanoma)
Isochromosome 1q
markers
A2058 1q-loss c1
Loss of 1q
markers
B
A2780 (ovarian cancer)
Chr12/1q Translocation
A2780 1q-loss c4
Loss of 1q
C
AGS (gastric cancer)
Chr8/1q Translocation
markers
AGS 1q-loss c11
Loss of 1q
markers

Figure S4. G-banded karyotypes of 1q-disomic clones.

(A) G-banded karyotypes of A2058 and a 1q-disomic A2058 clone. The third copy of chromosome 1q in A2058 is present as an isochromosome [chr 1, iso(1q), del(1q)], and 1q-disomic clone has lost a copy of 1q from the intact chromosome 1.

(B) G-banded karyotypes of A2780 and a 1q-disomic A2780 clone. The third copy of chromosome 1q in A2780 is translocated to chromosome 12q, and the 1q-disomic clone has lost this translocated copy of 1q.

(C) G-banded karyotypes of AGS and a 1q-disomic AGS clone. The third copy of chromosome 1q in AGS is translocated to chromosome 8p, and the 1q-disomic clone has lost a copy of 1q from an intact chromosome 1.

For all G-banded karyotypes in A-C, green arrows indicate the extra copy of chromosome 1q in parental cells and purple arrows indicate the deletion in the 1q-disomic clones.

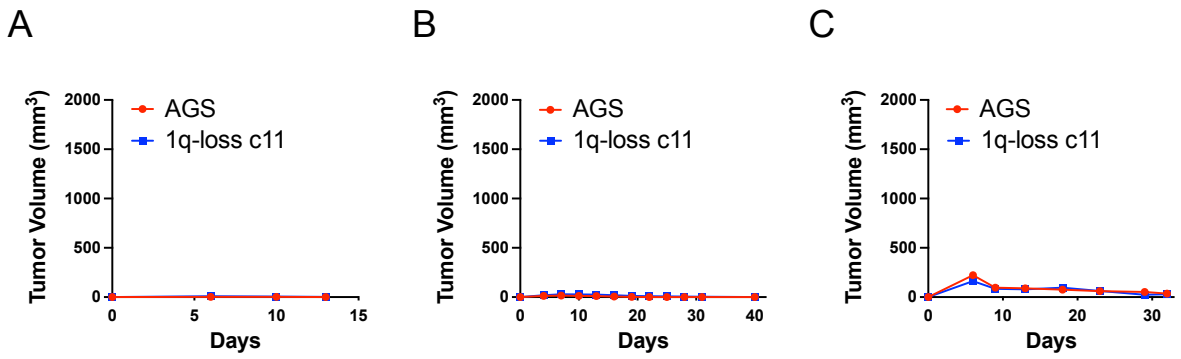
A
B
C
AGS
1q-loss c11
Tumor Volume (mm3)
Days
2000
1500
1000
500
0
0
5
10
15
20
30
40

Figure S5. Wild-type AGS cells fail to grow as subcutaneous xenografts.

(A) 5 million 1q-trisomic or 1q-disomic AGS cells were suspended in PBS and injected subcutaneously and contralaterally into 5-week-old female Nu/J mice. No tumor formation was observed.

(B) 4 million 1q-trisomic or 1q-disomic AGS cells were suspended in PBS and injected subcutaneously and contralaterally into 6-week-old female NSG mice. No tumor formation was observed.

(C) 15 million 1q-trisomic or 1q-disomic AGS cells were suspended in a 1:1 mixture of PBS and Matrigel and injected subcutaneously and contralaterally into 6-week-old female J:NU mice. No tumor formation was observed.

For all tumor growth curves in A-C, the graphs display the mean ± SEM for each trial. As no tumor formation was observed, the error bars do not extend beyond the data symbols.

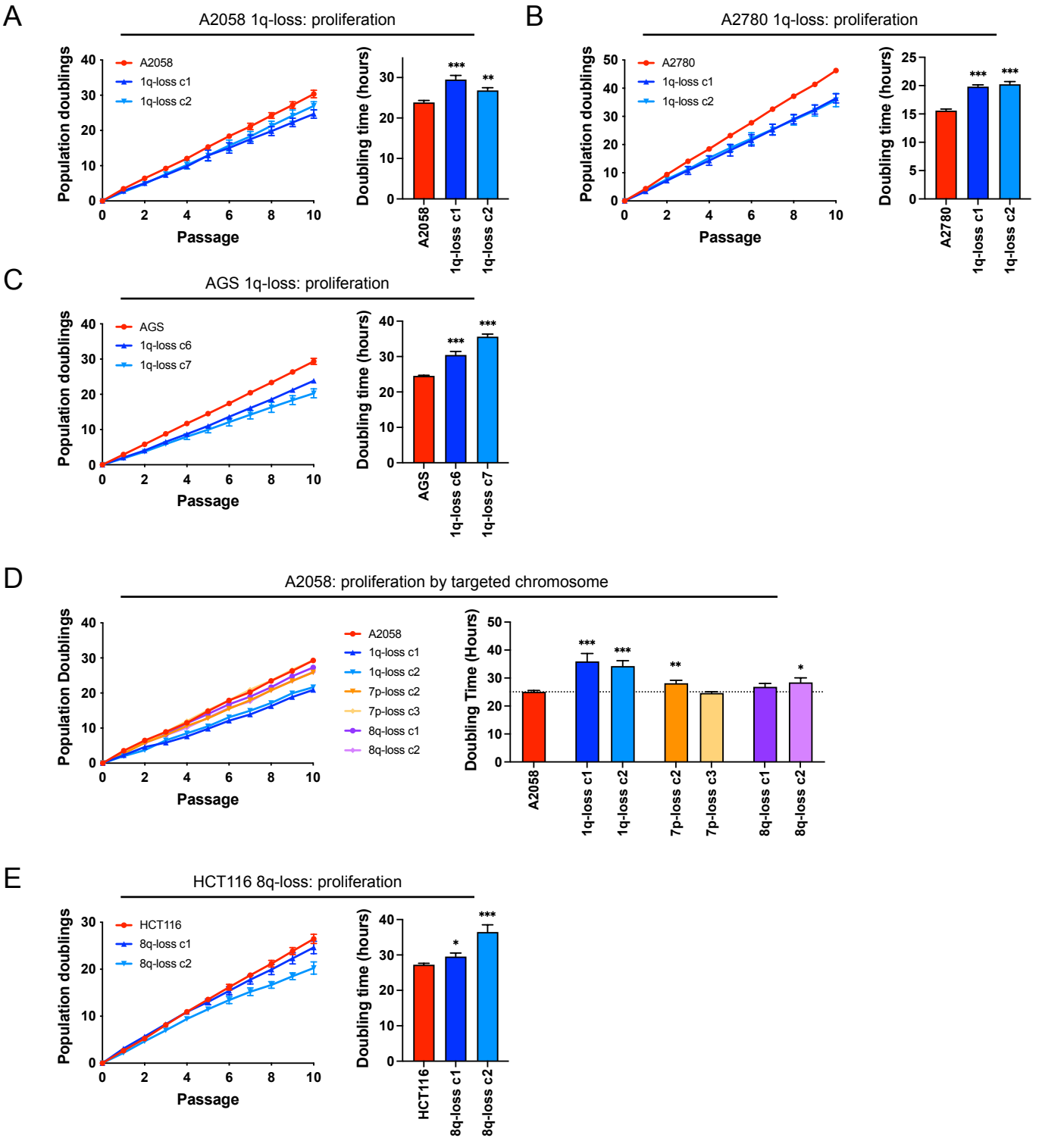
A
A2058 1q-loss: proliferation
Population doublings
A2058
1q-loss c1
1q-loss c2
Passage
Doubling time (hours)
***
**
A2058
1q-loss c1
1q-loss c2
B
A2780 1q-loss: proliferation
Population doublings
A2780
1q-loss c1
1q-loss c2
Passage
Doubling time (hours)
***
***
A2780
1q-loss c1
1q-loss c2
C
AGS 1q-loss: proliferation
Population doublings
AGS
1q-loss c6
1q-loss c7
Passage
Doubling time (hours)
***
***
AGS
1q-loss c6
1q-loss c7
D
A2058: proliferation by targeted chromosome
Population Doublings
A2058
1q-loss c1
1q-loss c2
7p-loss c2
7p-loss c3
8q-loss c1
8q-loss c2
Passage
Doubling Time (Hours)
***
***
**
*
A2058
1q-loss c1
1q-loss c2
7p-loss c2
7p-loss c3
8q-loss c1
8q-loss c2
E
HCT116 8q-loss: proliferation
Population doublings
HCT116
8q-loss c1
8q-loss c2
Passage
Doubling time (hours)
*
***
HCT116
8q-loss c1
8q-loss c2

Figure S6. Elimination of trisomy-1q causes a moderate decrease in 2D cell proliferation.

(A) Proliferation assays in 1q-trisomic and 1q-disomic A2058 cells.

(B) Proliferation assays in 1q-trisomic and 1q-disomic A2780 cells.

(C) Proliferation assays in 1q-trisomic and 1q-disomic AGS cells.

(D) Proliferation assays in parental and 1q-disomic, 7p-disomic, or 8q-disomic A2058 cells.

(E) Proliferation assays in 8q-trisomic and 8q-disomic HCT116 cells.

For all proliferation assays in A-E, cumulative population doublings are shown on the left, and the doubling time calculated from these assays is shown on the right. For the cumulative population doubling graphs, each point displays the mean ± SEM for each passage. The bar graphs of doubling time display the mean ± SEM, n=10 passages. Data were analyzed by unpaired t-test.

*$p < 0.05$, **$p < 0.005$, ***$p < 0.0005$

Supplementary Figure 7

C

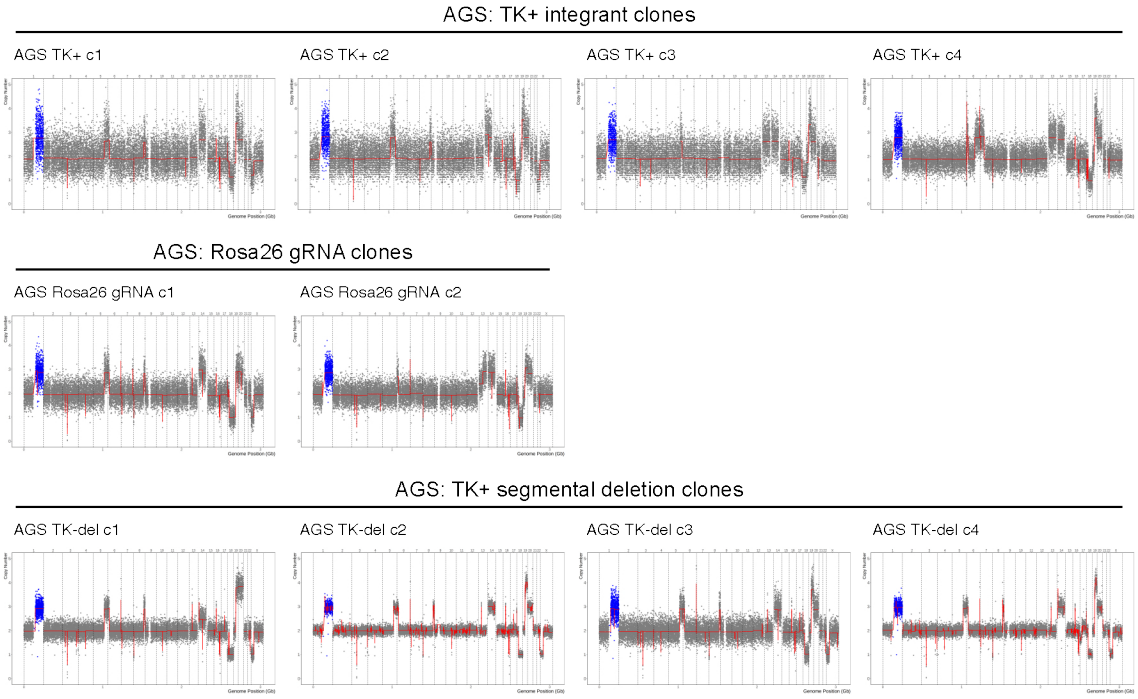
AGS: TK+ integrant clones
AGS TK+ c1
AGS TK+ c2
AGS TK+ c3
AGS TK+ c4
AGS: Rosa26 gRNA clones
AGS Rosa26 gRNA c1
AGS Rosa26 gRNA c2
AGS: TK+ segmental deletion clones
AGS TK-del c1
AGS TK-del c2
AGS TK-del c3
AGS TK-del c4

Figure S7. Karyotypes of control clones subjected to various CRISPR manipulations.

(A) SMASH karyotypes of the control clones generated from the 1q-trisomic cancer cell line A2058, with all clones maintaining 1q trisomy.

(B) SMASH karyotypes of the control clones generated from the 1q-trisomic cancer cell line A2780, with all clones maintaining 1q trisomy.

(C) SMASH karyotypes of the control clones generated from the 1q-trisomic cancer cell line AGS, with all clones maintaining 1q trisomy.

For all karyotypes in A-C, chromosome 1q is highlighted in blue. Additional information on how these clones were generated is presented in Figure S8.

Supplementary Figure 8

A

Type	Manipulation
TK+ Integrant Control	TK selection cassette integrated on chromosome to be eliminated, no gcv selection, retention of parental karyotype confirmed by SMASH
TK+ Segmental Deletion	Deletion of the TK selection cassette, gcv selection, retention of parental karyotype confirmed by SMASH
Rosa26 gRNA Control	Transfected with CRISPR gRNA targeting Rosa26 locus, retention of parental karyotype confirmed by SMASH
1q gRNA Control	Transfected with CRISPR gRNA targeting centromere-proximal region on Chr 1q, lesion repaired without arm loss, retention of 1q trisomy confirmed by SMASH
7p gRNA Control	Transfected with CRISPR gRNA targeting centromere-proximal region on Chr 7p, lesion repaired without arm loss, retention of 7p trisomy confirmed by SMASH
8q gRNA Control	Transfected with CRISPR gRNA targeting centromere-proximal region on Chr 8q, lesion repaired without arm loss, retention of 8q trisomy confirmed by SMASH
1q Telomere Truncation Control	Deletion of terminal genes from cytoband 1q44 to the end of the chromosome, retention of 1q trisomy confirmed by SMASH
Olfactory Receptor Gene Segmental Del: OR6K6 $^{+/+/KO}$	Deletion of a single copy of the olfactory receptor OR6K6, retention of 1q trisomy confirmed by SMASH
Olfactory Receptor Gene Segmental Del: OR2M4 $^{+/+/KO}$	Deletion of a single copy of the olfactory receptor OR2M4, retention of 1q trisomy confirmed by SMASH

B

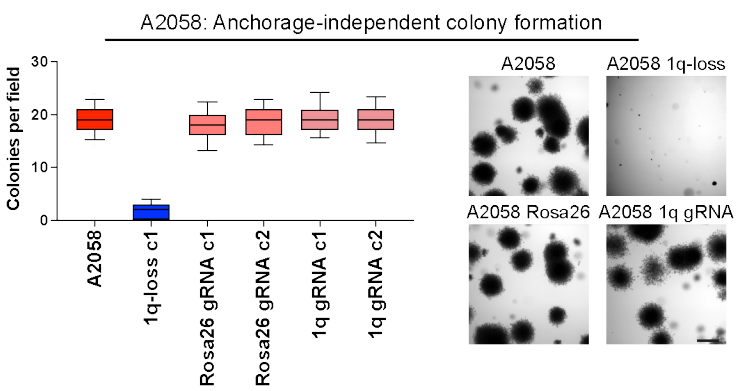

C

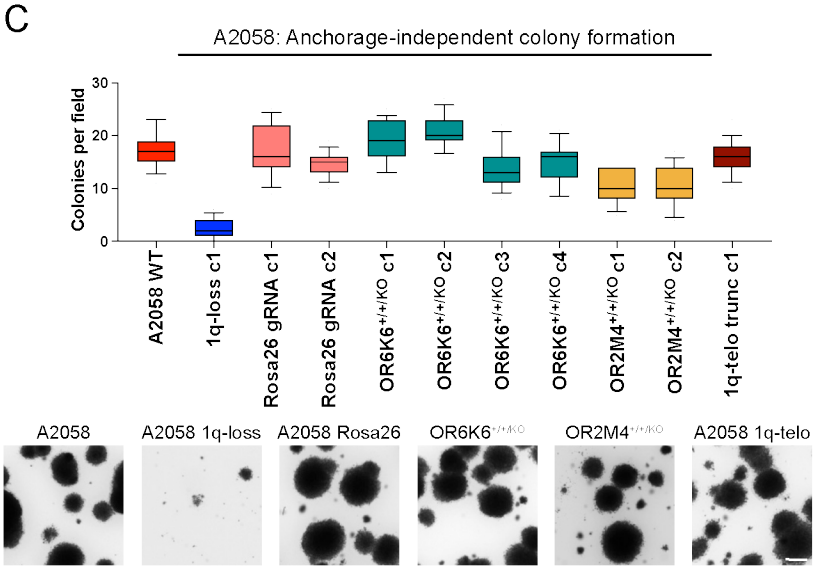

D

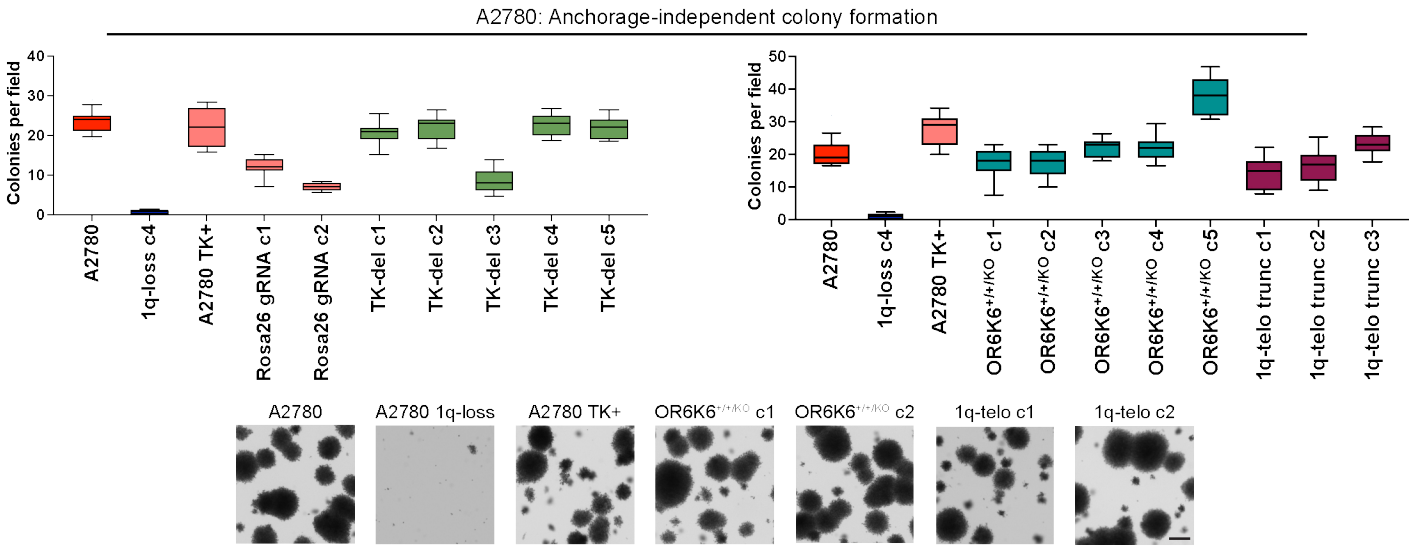

E

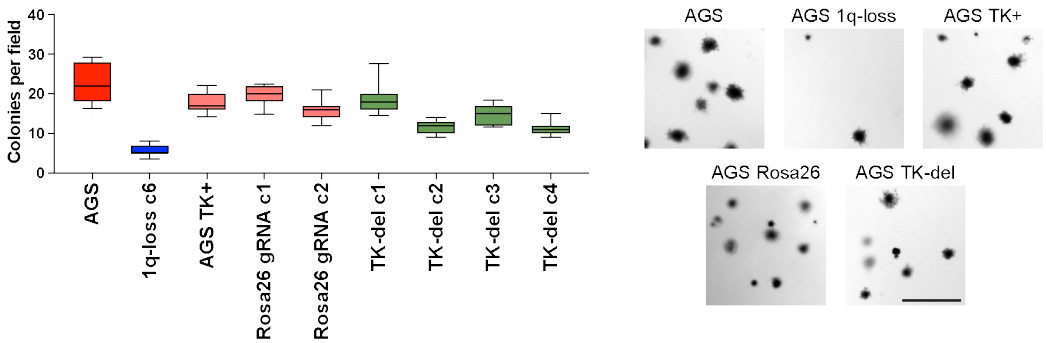

Figure S8. 1q-disomic cancer cells exhibit uniformly worse growth in soft agar compared to control clones subjected to various CRISPR manipulations.

(A) A schematic of the various strategies used to generate the control clones tested in this work. Note that the 7p and 8q gRNA control clones are tested in Figure S10.

(B) A 1q-disomic clone exhibits worse anchorage-independent growth compared to *Rosa26* gRNA and 1q gRNA control clones in A2058.

(C) A 1q-disomic clone exhibits worse anchorage-independent growth compared to *Rosa26* gRNA, olfactory receptor deletion, and 1q-telo truncation control clones in A2058.

(D) A 1q-disomic clone exhibits worse anchorage-independent growth compared to TK+ integrant, *Rosa26* gRNA, TK-segmental deletion, olfactory receptor deletion, and 1q-telo truncation control clones in A2780. Note that these control clones display some variation in anchorage-independent growth, but every control clone grew better than a 1q-disomic clone.

(E) A 1q-disomic clone exhibits worse anchorage-independent growth compared to TK+ integrant, *Rosa26* gRNA, and TK-segmental deletion control clones in AGS.

For anchorage-independent growth assays in B-E, boxes represent the 25th, 50th, and 75th percentiles of colonies per field, while the whiskers represent the 10th and 90th percentiles. Data are from n = 15 fields of view, and a representative trial is shown for each experiment (n ≥ 2 total trials). Scale bars = 250 μm.

Supplementary Figure 9

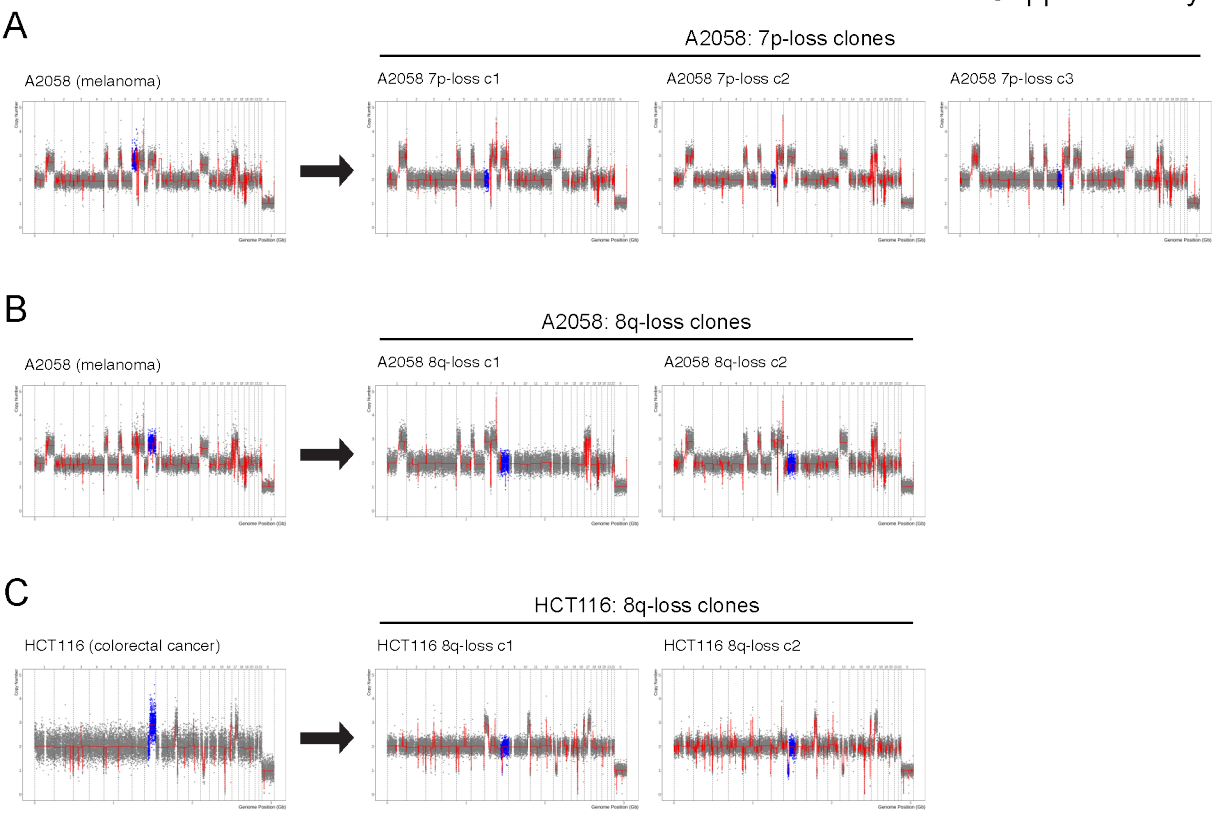

Figure S9. Additional karyotypes of 7p-disomic and 8q-disomic clones.

(A) SMASH karyotypes of 7p-disomic clones generated from the 7p-trisomic cancer cell line A2058. Chromosome 7p is highlighted in blue.

(B) SMASH karyotypes of 8q-disomic clones generated from the 8q-trisomic cancer cell line A2058. Chromosome 8q is highlighted in blue.

(C) SMASH karyotypes of 8q-disomic clones generated from the 8q-trisomic cancer cell line HCT116. Chromosome 8q is highlighted in blue.

Supplementary Figure 10

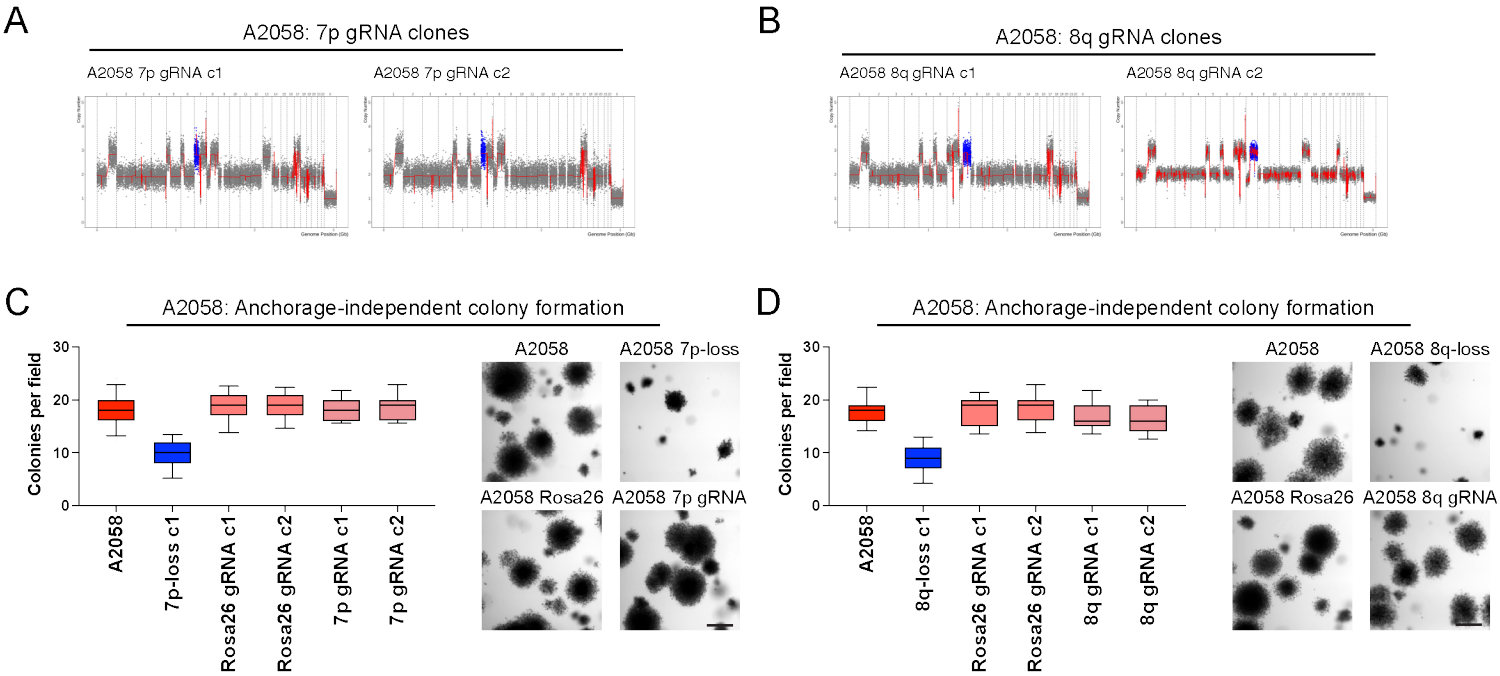

Figure S10. Karyotypes and anchorage-independent growth of A2058 7p and 8q control clones

(A) SMASH karyotypes of control clones generated by transfecting cells with the same CRISPR gRNA used to produce the 7p-disomic clones. Clones were selected that maintain the 7p trisomy. Chromosome 7p is highlighted in blue.

(B) SMASH karyotypes of control clones generated by transfecting cells with the same CRISPR gRNA used to produce the 8q-disomic clones. Clones were selected that maintain the 8q trisomy. Chromosome 8q is highlighted in blue.

(C) A 7p-disomic clone exhibits worse anchorage-independent growth compared to *Rosa26* gRNA and 7p gRNA control clones in A2058.

(D) An 8q-disomic clone exhibits worse anchorage-independent growth compared to *Rosa26* gRNA and 8q gRNA control clones in A2058.

For anchorage-independent growth assays in C-D, boxes represent the 25th, 50th, and 75th percentiles of colonies per field, while the whiskers represent the 10th and 90th percentiles. Unpaired t-test, n = 15 fields of view, data from representative trial (n ≥ 2 total trials). Representative images are shown next to each graph. Scale bars = 250 μm.

Supplementary Figure 11

A

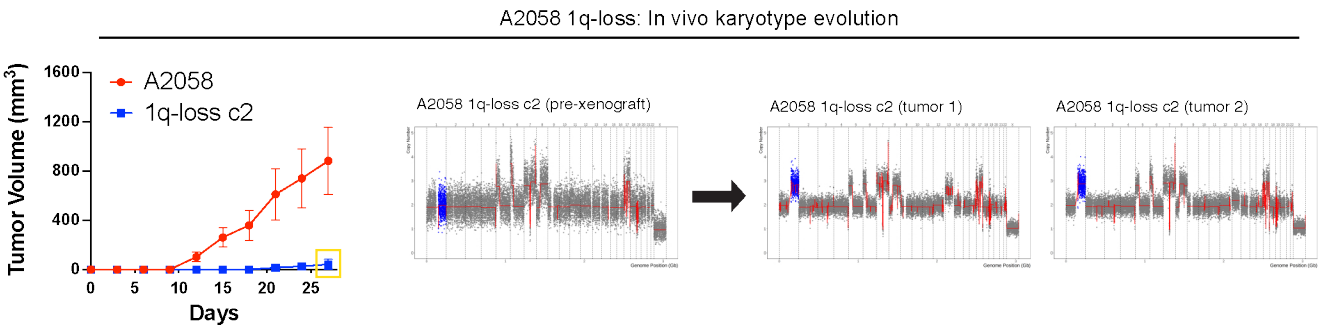

B

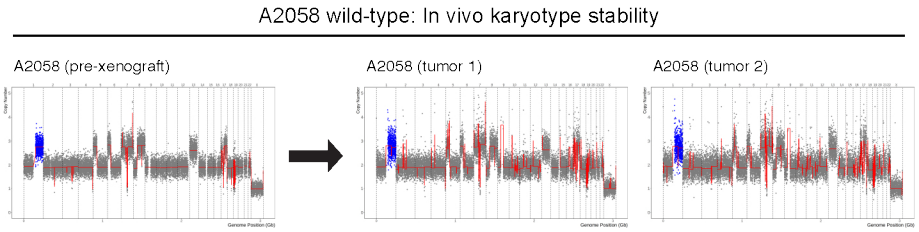

Figure S11. Karyotype analysis of additional 1q-trisomic and 1q-disomic A2058 xenografts.

(A) 1q-disomic cells frequently evolve to recover a third copy of chromosome 1q during xenograft growth.

(B) A2058 wildtype tumors exhibit karyotypic stability during xenograft growth.

For the data shown in A-B, initial karyotypes for these lines prior to xenograft assays are shown on the left, and karyotypes of tumors following the xenograft assays are shown on the right. Chromosome 1q is highlighted in blue.

Supplementary Figure 12

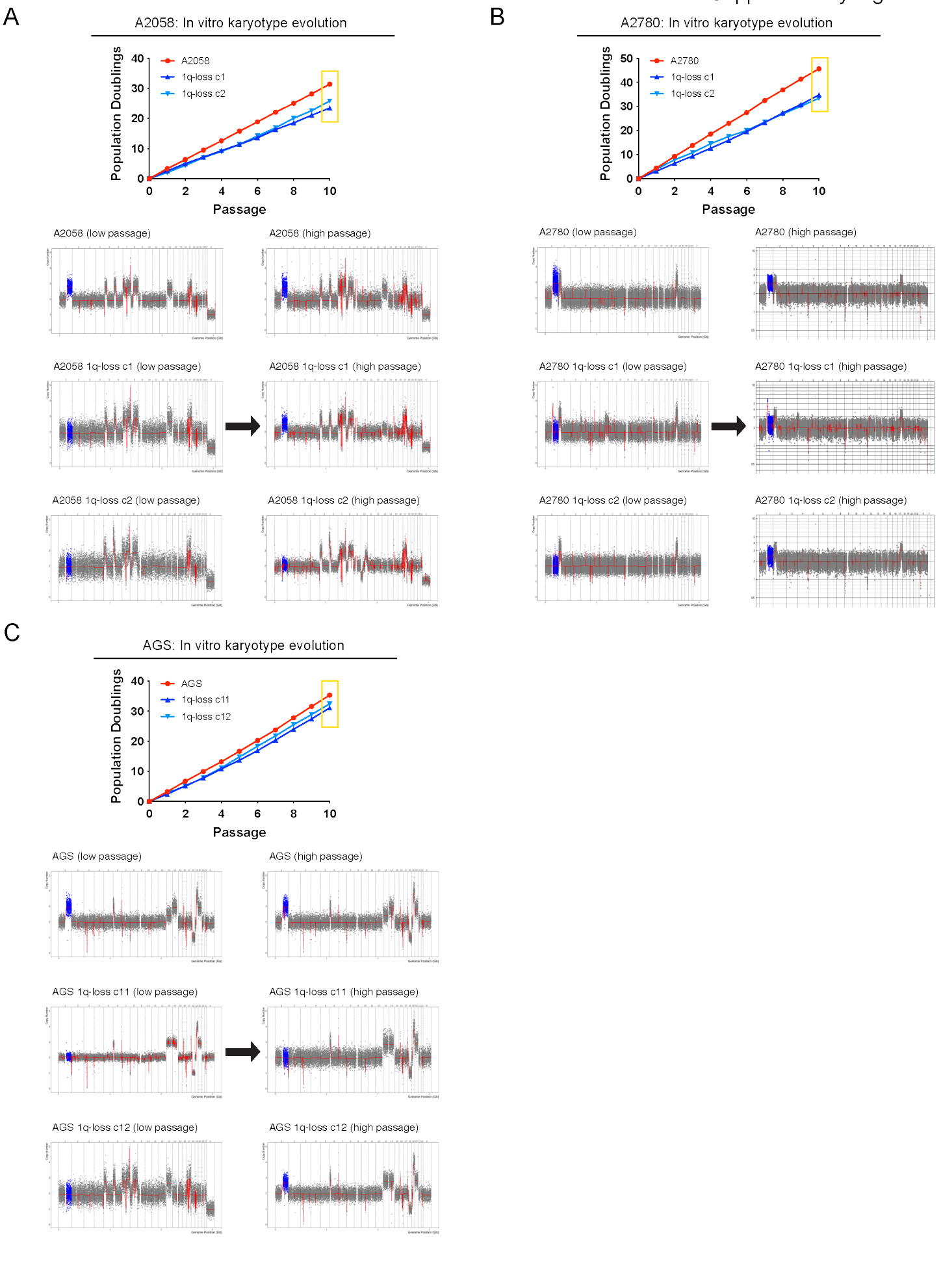

Figure S12. Karyotype evolution of 1q-disomic cancer cells following serial passaging in vitro.

(A) Regain of the 1q trisomy during prolonged in vitro passaging of A2058 1q-disomic clones.

(B) Regain of the 1q trisomy during prolonged in vitro passaging of A2780 1q-disomic clones.

(C) Regain of the 1q trisomy during prolonged in vitro passaging of AGS 1q-disomic clones.

For A-C, cells were harvested at the start of the proliferation assay and after 10 passages at the conclusion of the assay, and subject to SMASH karyotyping. Karyotypes are shown below, with chromosome 1q highlighted in blue.

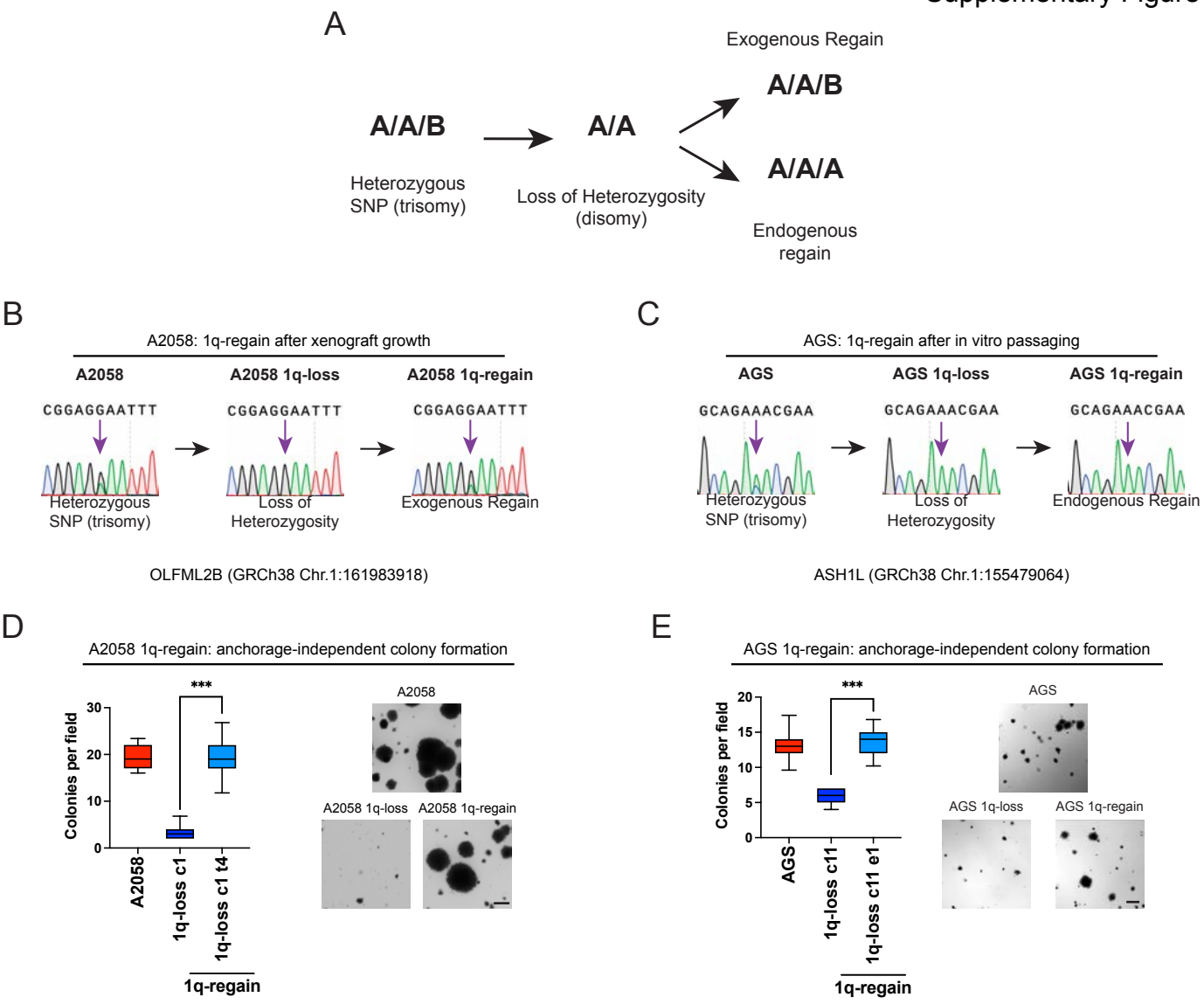
A
Exogenous Regain
A/A/B
A/A/B
A/A
A/A/A
Heterozygous SNP (trisomy)
Loss of Heterozygosity (disomy)
Endogenous regain
B
A2058: 1q-regain after xenograft growth
A2058
A2058 1q-loss
A2058 1q-regain
CGGAGGAATTT
Heterozygous SNP (trisomy)
Loss of Heterozygosity
Exogenous Regain
OLFML2B (GRCh38 Chr.1:161983918)
C
AGS: 1q-regain after in vitro passaging
AGS
AGS 1q-loss
AGS 1q-regain
GCAGAAACGAA
Heterozygous SNP (trisomy)
Loss of Heterozygosity
Endogenous Regain
ASH1L (GRCh38 Chr.1:155479064)
D
A2058 1q-regain: anchorage-independent colony formation
Colonies per field
***
A2058
1q-loss c1
1q-loss c1 t4
1q-regain
A2058
A2058 1q-loss
A2058 1q-regain
E
AGS 1q-regain: anchorage-independent colony formation
Colonies per field
***
AGS
1q-loss c11
1q-loss c11 e1
1q-regain
AGS
AGS 1q-loss
AGS 1q-regain

Figure S13. Identifying the source of the 1q-regain events during cellular evolution.

(A) A schematic of our approach to use SNP sequencing to uncover how 1q-regain events occur. Using published whole-exome sequencing data, we identified SNPs encoded on chromosome 1q that were heterozygous in the starting trisomic population. We sequenced these same loci following aneuploidy-loss and identified SNPs that underwent LOH. Then, we sequenced these LOH-SNPs following 1q-regain. We reasoned that if 1q regain occurred to the missegregation or duplication of an endogenous copy of chromosome 1q, then LOH should be maintained at these loci. In contrast, if heterozygosity was restored, then that was evidence that the 1q-disomic cell population had been outcompeted by an exogenous population of trisomic cells.

(B) An example of an exogenous regain event in A2058 1q-loss cells that were grown as a xenograft.

(C) An example of an endogenous regain event in AGS 1q-loss cells that were passaged in culture for 30 days.

(D) 1q-regain correlates with improved anchorage-independent growth in A2058 cells.

(E) 1q-regain correlates with improved anchorage-independent growth in AGS cells.

For the anchorage-independent growth assays in D and E, the boxes represent the 25th, 50th, and 75th percentiles of colonies per field, while the whiskers represent the 10th and 90th percentiles. Unpaired t-test, n = 15 fields of view, data from representative trial (n ≥ 2 total trials). Representative images are shown on the right. Scale bars = 250 μm.

***$p < 0.0005$

Supplementary Figure 14

A

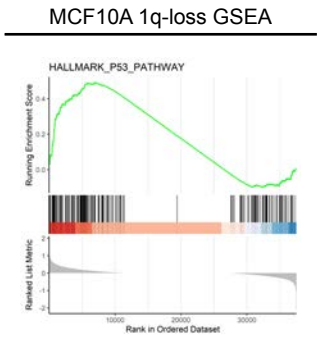

B

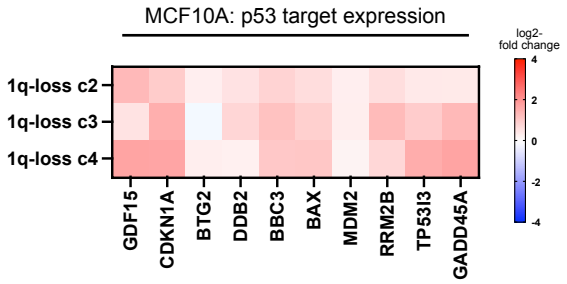

C

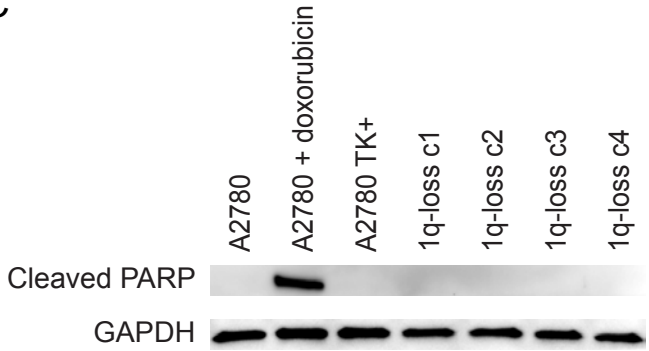

D

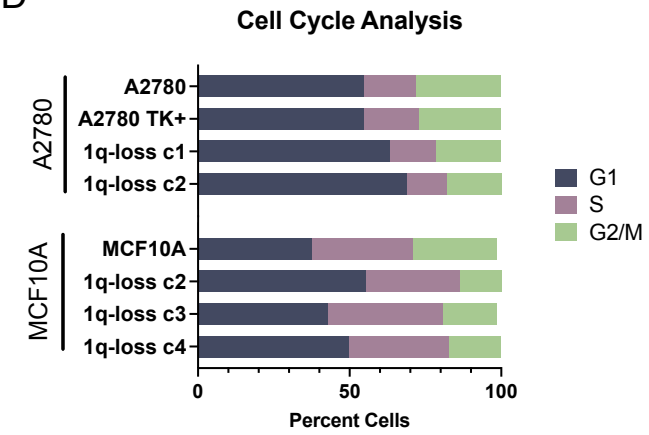

E

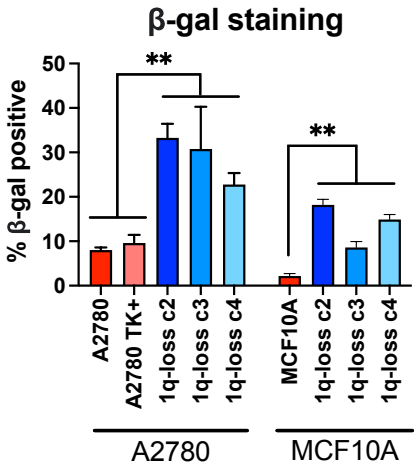

F

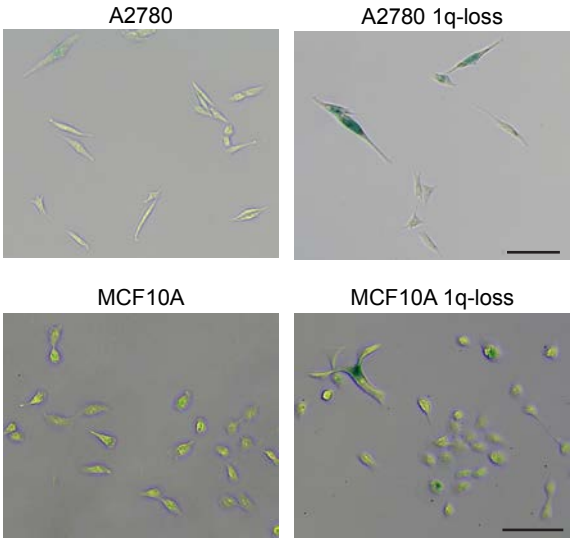

Figure S14. Elimination of the 1q trisomy causes a G1 delay and an increase in senescence.

(A) GSEA analysis of MCF10A RNA-seq data reveals upregulation of the p53 pathway in the 1q-disomic clones, relative to the parental trisomy.

(B) A heatmap displaying the upregulation of 10 p53 target genes in MCF10A 1q-disomic clones.

(C) Aneuploidy-loss does not trigger apoptosis. Amounts of cleaved PARP1 were assessed using western blotting to determine whether aneuploidy-loss induces apoptosis. As a positive control, wild-type cells were treated with the DNA-damaging agent doxorubicin. GAPDH was analyzed as a loading control.

(D) Cell cycle analysis of A2780 and MCF10A wild-type and 1q-disomic clones, determined via propidium iodide staining. Data from representative trials are shown (n = 2 total trials).

(E) Analysis of senescence in A2780 and MCF10A wild-type and 1q-disomic clones, determined via staining for beta-galactosidase. Mean ± SEM, n=2 trials.

(F) Images of cells analyzed in (E). Scale bars = 50 μm.

Supplementary Figure 15

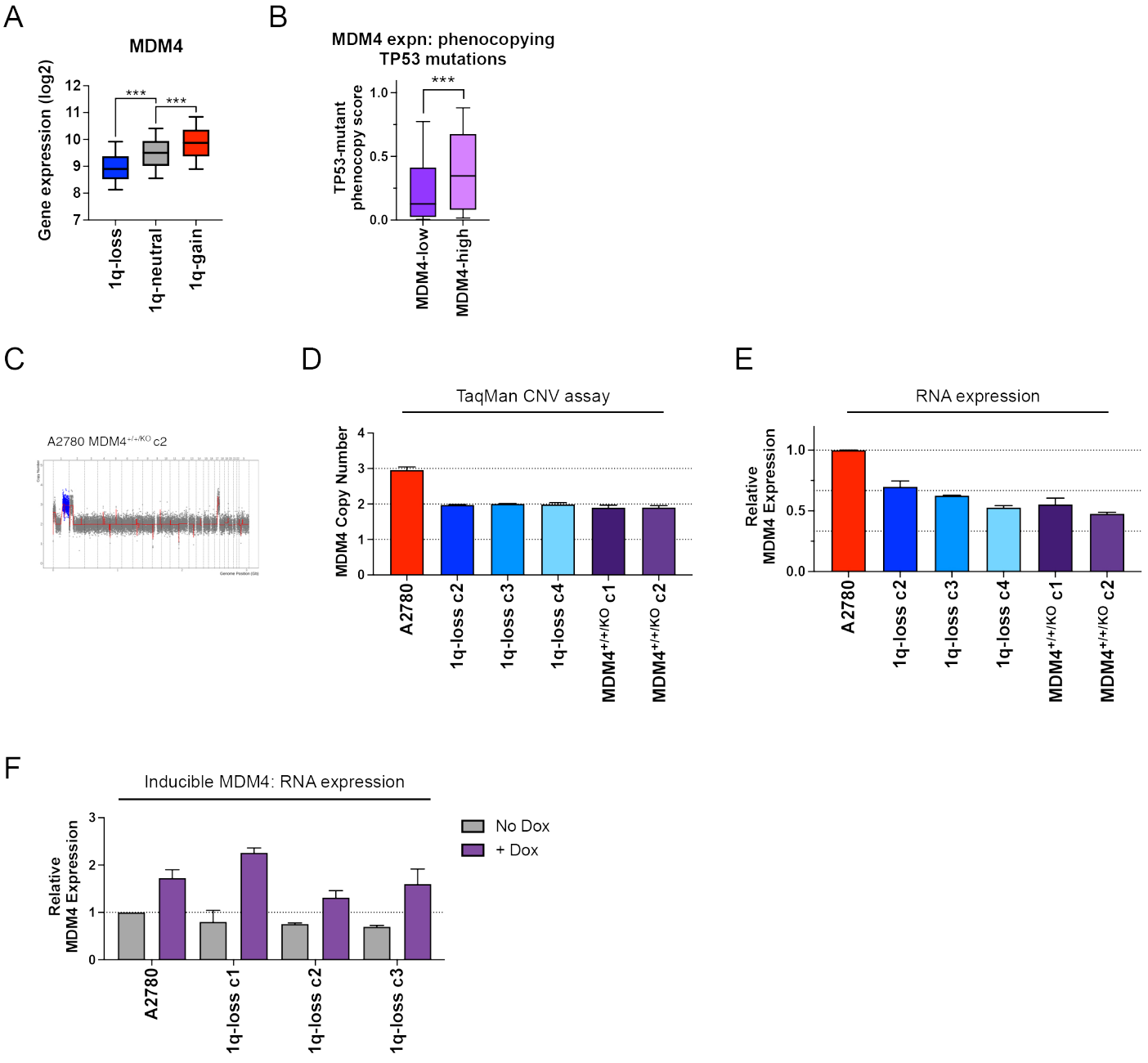

Figure S15. *MDM4* expression in human tumors and *MDM4* genetic manipulations in A2780 cells.

(A) Boxplots displaying the expression of *MDM4* in human cancers from TCGA split based on the copy number of chromosome 1q. Data were analyzed using unpaired t-tests.

(B) Boxplots displaying the *TP53*-mutation phenocopy signature (*45*) in cancers from TCGA, split based on the expression of *MDM4*. Only *TP53*-wildtype cancers are included in this analysis.

(C) SMASH karyotype demonstrating maintenance of the chromosome 1q trisomy in an $MDM4^{+/+/KO}$ clone. Chromosome 1q is highlighted in blue.

(D) TaqMan copy number verification of the deletion of a single copy of *MDM4* in A2780 cells. Mean ± SEM, n=2 probes for *MDM4*.

(E) $MDM4^{+/+/KO}$ and 1q-disomic clones exhibit decreased expression of *MDM4*, as determined through TaqMan gene expression assays. Data are normalized to parental A2780.

(F) Expression of *MDM4* in 1q-trisomic and 1q-disomic cells harboring *MDM4* under the control of a doxycycline-inducible promoter. *MDM4* expression was measured using qRT-PCR. Mean ± SEM, n=2 trials.

***$p < 0.0005$

Supplementary Figure 16

A

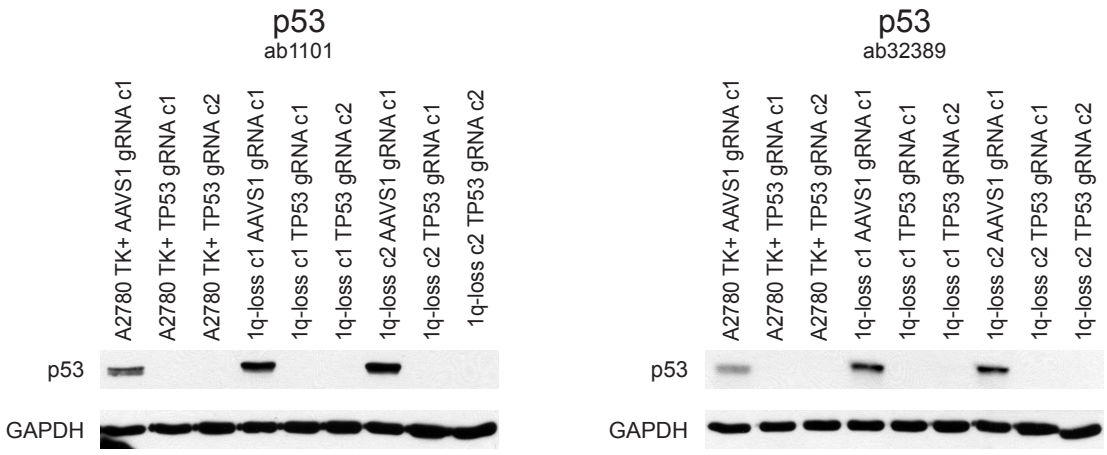

B

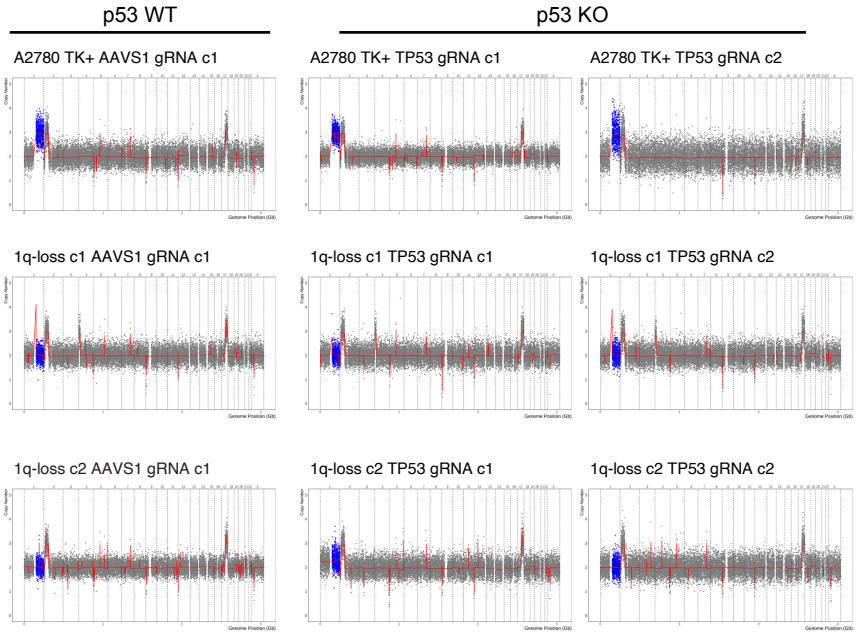

C

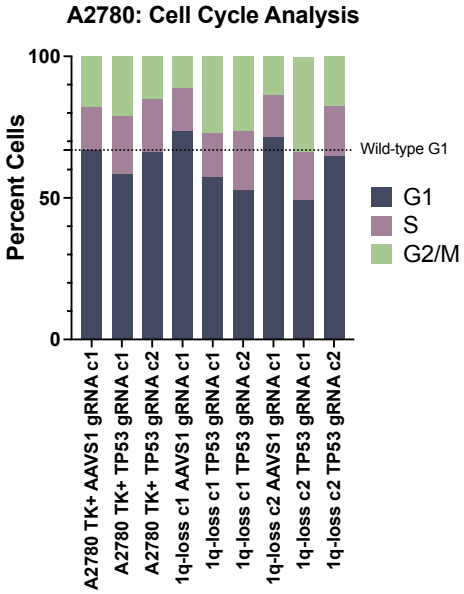

D

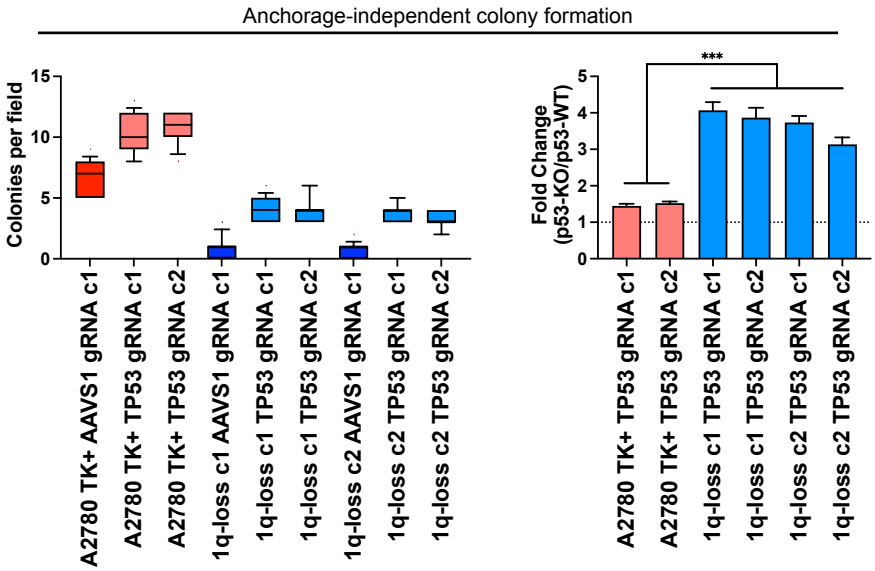

Figure S16. Deletion of *TP53* selectively increases the fitness of 1q-disomic cells.

(A) Western blot validation of p53-KO with two different antibodies. *AAVS1* gRNA clones serve as isogenic p53-WT controls. GAPDH was used as a loading control.

(B) SMASH karyotypes of p53-KO and p53-WT clones. TK+ integrant clones maintain the 1q trisomy, 1q-disomic clones maintain the 1q disomy, and no other karyotypic alterations are observed. Chromosome 1q is highlighted in blue.

(C) Cell cycle analysis of p53-KO and p53-WT clones in A2780 TK+ and 1q-disomic lines, determined via propidium iodide staining. Data from representative trials are shown (n = 2 total trials).

(D) Deletion of *TP53* increases anchorage-independent growth by ~1.5-fold in 1q-trisomic clones and by ~4-fold in 1q-disomic clones. Boxes represent the 25th, 50th, and 75th percentiles of colonies per field, while the whiskers represent the 10th and 90th percentiles. Unpaired t-test, n = 15 fields of view, data from representative trial (n ≥ 2 total trials).

***$p < 0.0005$

Supplementary Figure 17

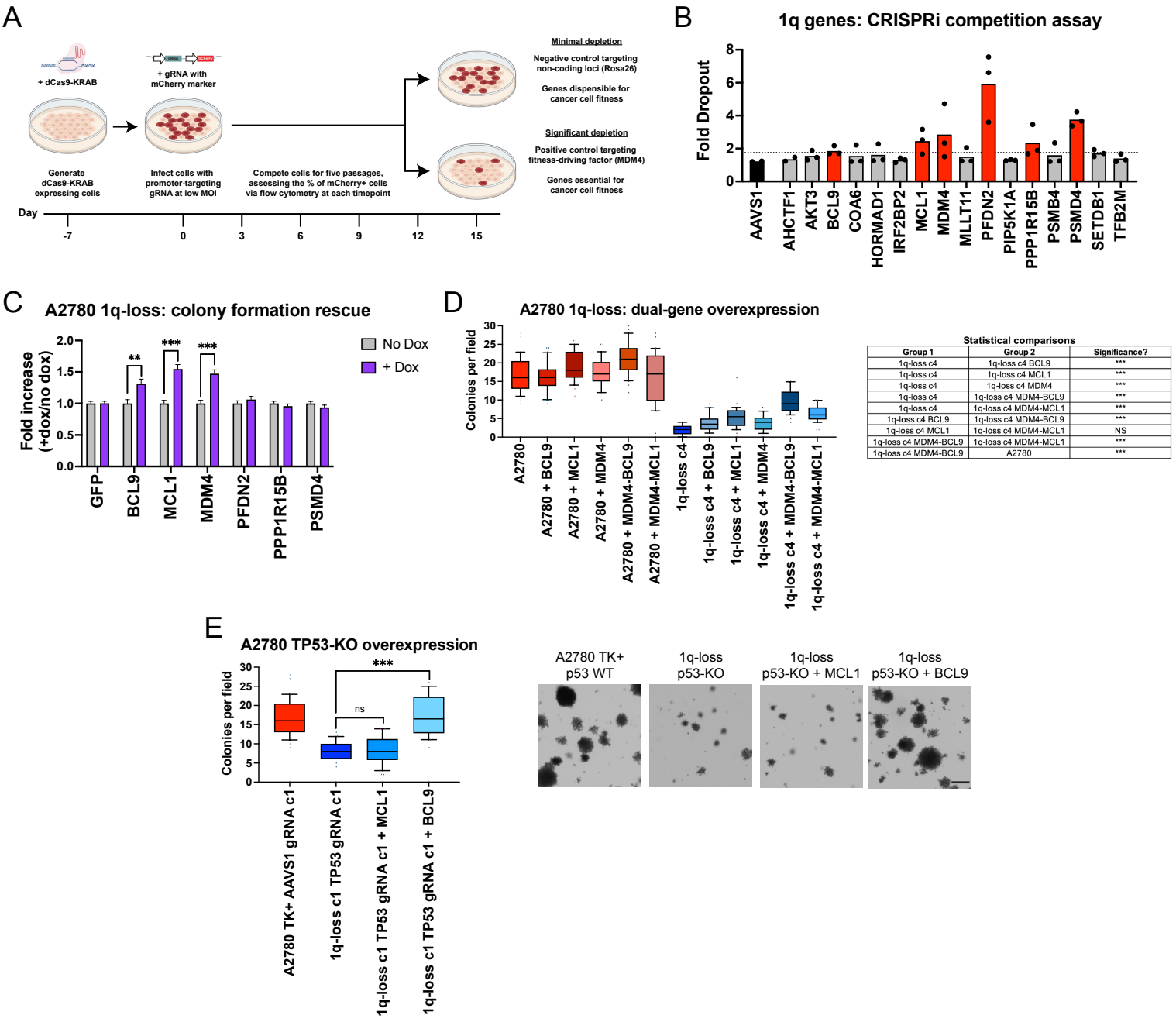

Figure S17. A screen to identify additional dosage-sensitive genes that promote malignant growth in 1q-trisomic cells.

(A) A schematic of the CRISPRi competition assay used to identify genes whose downregulation decreases fitness in 1q-trisomic A2780 cells. Adapted from (*48*).

(B) A bar graph displaying the mean dropout from the A2780 CRISPRi competition assay presented in (A). Guides targeting *AAVS1* were used as a negative control and guides targeting *MDM4* were used as a positive control. Black dots indicate dropout from individual gRNAs. A dotted line is plotted at 1.75-fold dropout, which was selected as a threshold to prioritize candidate genes for further study. gRNAs targeting six genes, indicated in red, exhibited a mean dropout greater than 1.75-fold in these assays.

(C) A bar graph displaying the effects of upregulating different genes on anchorage-independent growth in A2780 1q-disomic clones. 1q-disomic clones were transduced with lentiviruses encoding the indicated cDNAs under the control of a doxycycline-inducible promoter, and then the cells were plated in soft agar with or without doxycycline. A cDNA encoding *GFP* was included as a negative control. Three genes – *BCL9*, *MCL1*, and *MDM4* – were sufficient to increase anchorage-independent growth when overexpressed. Mean ± SEM, 4 clones x 15 independent fields of view were analyzed for each gene.

(D) Boxplots displaying the growth of A2780 1q-trisomic or 1q-disomic cells overexpressing the indicated gene or genes. The table on the right indicates significance tests for this experiment.

(E) Boxplots displaying the growth of A2780 1q-trisomic or 1q-disomic cells overexpressing the indicated gene. The micrographs display representative images of colony formation for 1q-trisomic and 1q-disomic clones.

For the graphs in D and E, the boxplots represent the 25th, 50th, and 75th percentiles of the indicated data, while the whiskers represent the 10th and 90th percentiles of the indicated data. For the soft agar experiments in D and E, the data are from n = 30 fields of view. Data are from a representative trial (n ≥ 2 total trials). Scale bars = 250 μm.

Supplementary Figure 18

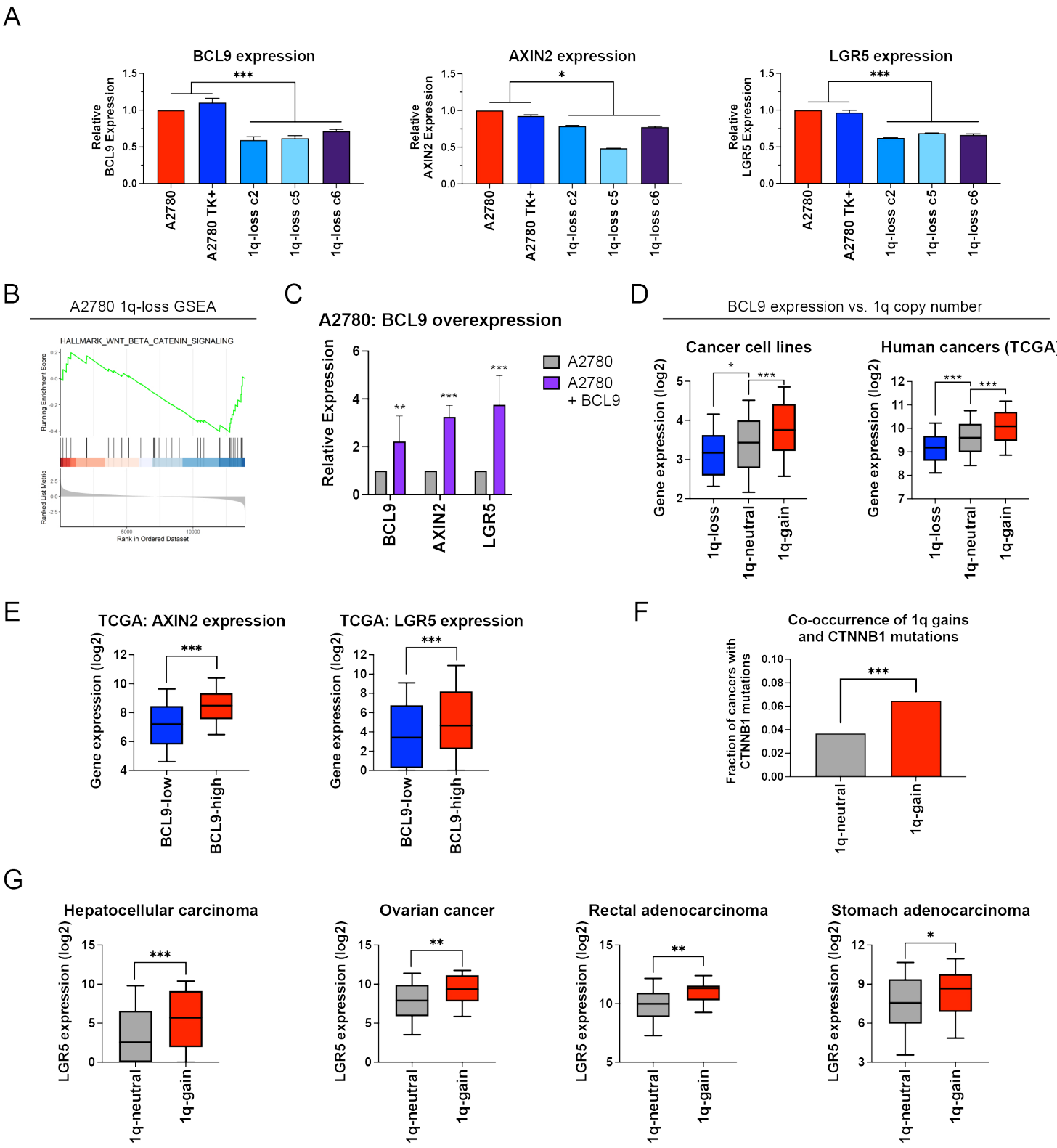

Figure S18. *BCL9* expression enhances Wnt/β-catenin signaling in 1q-trisomic cancers.

(A) 1q-disomic clones exhibit lower levels of *BCL9*, *AXIN2*, and *LGR5*. Mean ± SEM, 2 independent replicates.

(B) GSEA analysis of A2780 RNA-seq data reveals downregulation of the Wnt/β-catenin pathway in the 1q-disomic clones, relative to the parental trisomy.

(C) A2780 cells overexpressing *BCL9* exhibit higher levels of *AXIN2* and *LGR5*. Mean ± SEM, 3 independent replicates.

(D) Boxplots displaying the expression of *BCL9* from the cancer cell line encyclopedia (left) and TCGA (right), divided based on the copy number of chromosome 1q. The boxplots represent the 25th, 50th, and 75th percentiles of the indicated data, while the whiskers represent the 10th and 90th percentiles of the indicated data. Data were analyzed using unpaired t-tests. N = 10,331 samples from TCGA, and 942 samples from CCLE.

(E) Boxplots displaying the expression of *AXIN2* and *LGR5* in cancers from TCGA, divided based the mean expression of *BCL9*. The boxplots represent the 25th, 50th, and 75th percentiles of the indicated data, while the whiskers represent the 10th and 90th percentiles of the indicated data. Data were analyzed using unpaired t-tests. N = 10,331 samples from TCGA.

(F) The fraction of cancers from TCGA with mutations in *CTNNB1*, divided based on whether the cancers are neutral for chromosome 1q or exhibit a gain of chromosome 1q. Data were analyzed using Fisher's exact test. N = 10,331 samples from TCGA.

(G) Boxplots displaying the expression of *LGR5* in cancers from TCGA, divided based on whether the cancers are neutral for chromosome 1q or exhibit a gain of chromosome 1q. The boxplots represent the 25th, 50th, and 75th percentiles of the indicated data, while the whiskers represent the 10th and 90th percentiles of the indicated data. Data were analyzed using unpaired t-tests. N = 10,331 samples from TCGA.

*$p < 0.05$, ** $p < 0.005$, *** $p < 0.0005$

Supplementary Figure 19

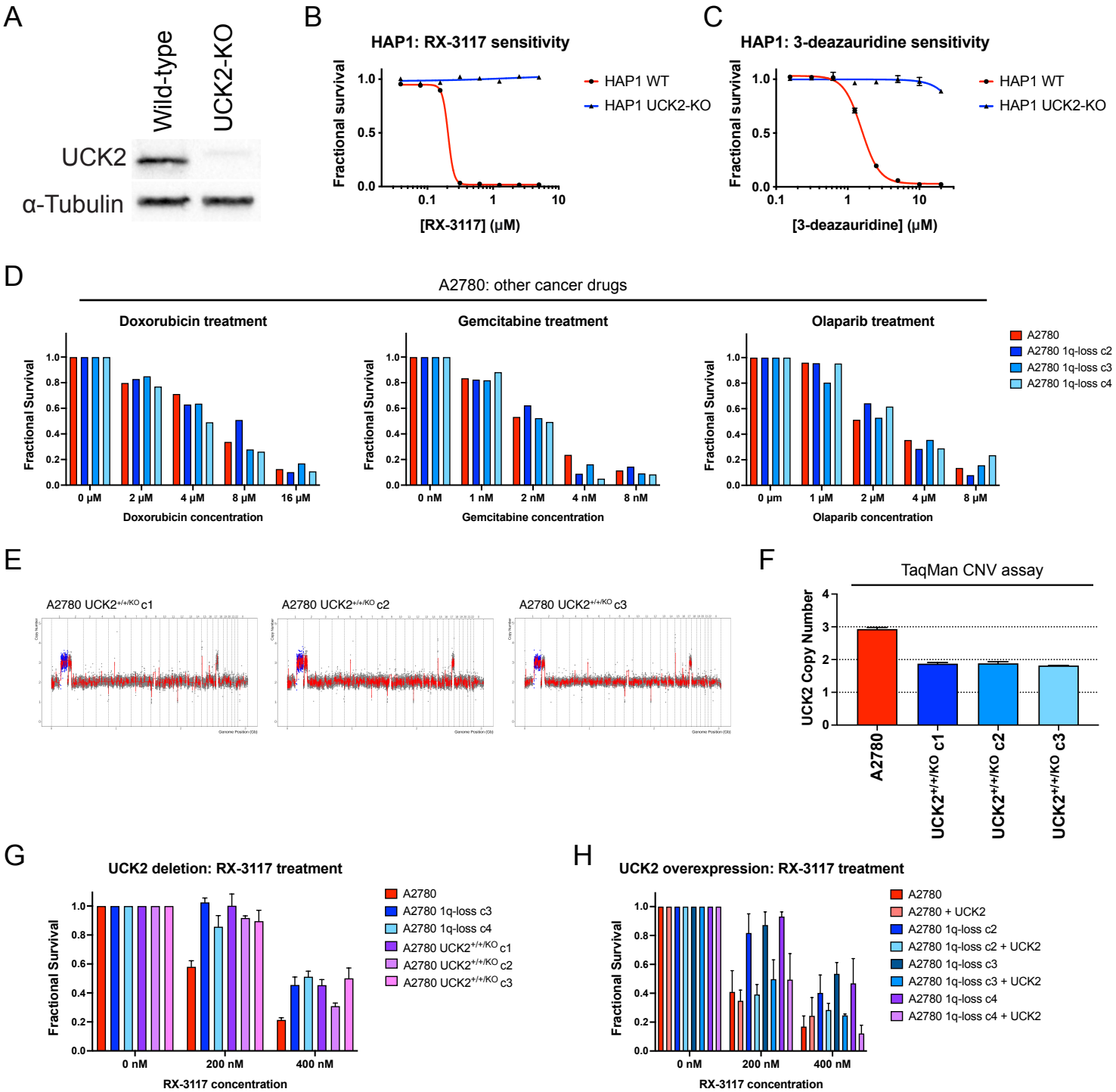

Figure S19. *UCK2* expression sensitizes cancer cells to RX-3117 and 3-deazauridine.

(A) Western blotting verifying lack of *UCK2* expression in the HAP1 *UCK2-KO* clone. Tubulin was used as a loading control.

(B) 7-point dose response curve displaying the viability of HAP1 and HAP1 *UCK2-KO* cells treated with varying concentrations of RX-3117.

(C) 7-point dose response curve displaying the viability of HAP1 and HAP1 *UCK2-KO* cells treated with varying concentrations of 3-deazauridine.

(D) Viability of A2780 cells treated with different concentrations of the indicated anti-cancer drug.

(E) SMASH karyotypes demonstrating maintenance of the chromosome 1q trisomy in $UCK2^{+/+/KO}$ clones. Chromosome 1q is highlighted in blue.

(F) TaqMan copy number verification of the deletion of a single copy of *UCK2* in A2780 cells. Mean ± SEM, n=2 probes for *UCK2*.

(G) Viability of A2780, A2780 1q-loss, and A2780 $UCK2^{+/+/KO}$ cells treated with RX-3117. Mean ± SEM, data from representative trials are shown (n ≥ 3 total trials).

(H) Viability of A2780, A2780 1q-loss, and A2780 cells transduced with *UCK2* cDNA treated with RX-3117. Mean ± SEM, data from representative trials are shown (n ≥ 3 total trials).

For the 7-point dose response curves in B-C, symbols represent the mean ± SEM. Data from representative trials are shown (n ≥ 3 total trials).

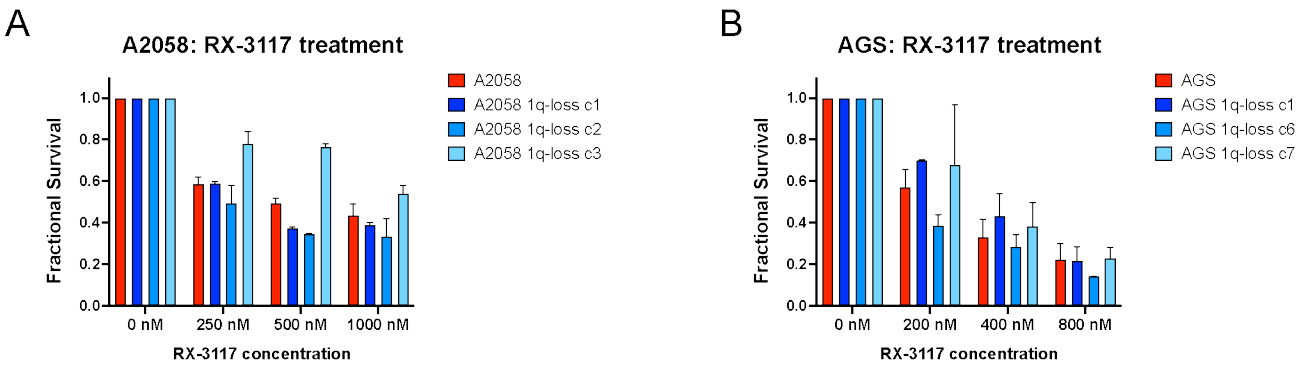
A
A2058: RX-3117 treatment
Fractional Survival
1.0
0.8
0.6
0.4
0.2
0.0
0 nM
250 nM
500 nM
1000 nM
RX-3117 concentration
A2058
A2058 1q-loss c1
A2058 1q-loss c2
A2058 1q-loss c3
B
AGS: RX-3117 treatment
Fractional Survival
0 nM
200 nM
400 nM
800 nM
RX-3117 concentration
AGS
AGS 1q-loss c1
AGS 1q-loss c6
AGS 1q-loss c7

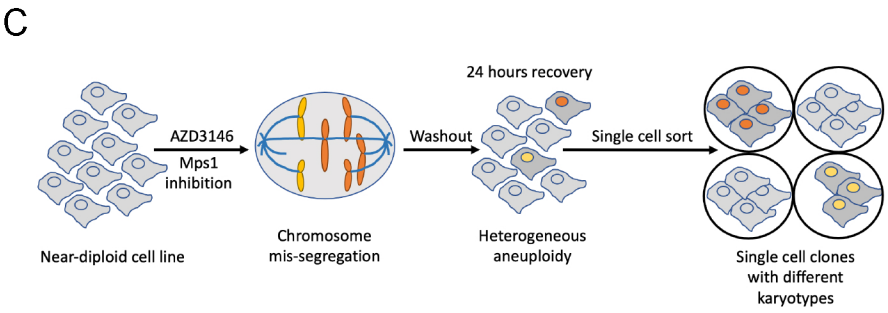
C
AZD3146
Mps1
inhibition
Washout
24 hours recovery
Single cell sort
Near-diploid cell line
Chromosome
mis-segregation
Heterogeneous
aneuploidy
Single cell clones
with different
karyotypes

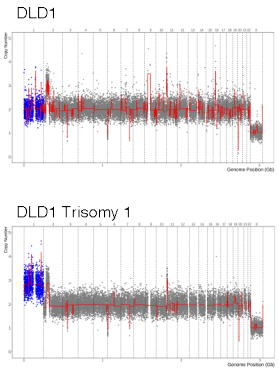
D
DLD1
DLD1 Trisomy 1

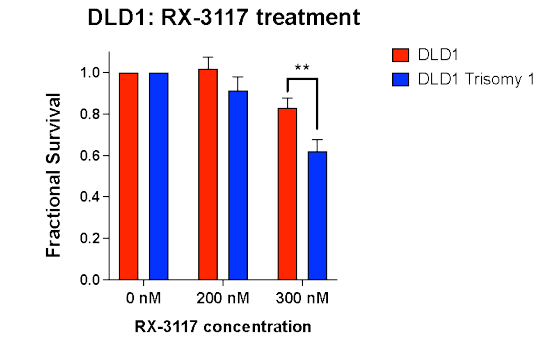
E
DLD1: RX-3117 treatment
Fractional Survival
1.0
0.8
0.6
0.4
0.2
0.0
**
0 nM
200 nM
300 nM
RX-3117 concentration
DLD1
DLD1 Trisomy 1

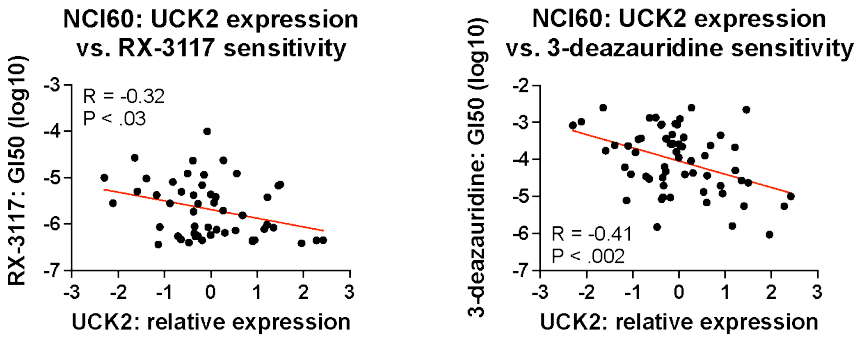
F
NCI60: UCK2 expression
vs. RX-3117 sensitivity
RX-3117: GI50 (log10)
R = -0.32
P < .03
-3
-4
-5
-6
-7
-3
-2
-1
0
1
2
3
UCK2: relative expression
NCI60: UCK2 expression
vs. 3-deazauridine sensitivity
3-deazauridine: GI50 (log10)
-2
-3
-4
-5
-6
-7
R = -0.41
P < .002
UCK2: relative expression

Figure S20. *UCK2* expression and sensitivity to RX-3117 and 3-deazauridine in other cell line models.

(A) Viability of A2058 and A2058 1q-loss cells treated with RX-3117. Mean ± SEM, data from representative trials are shown (n ≥ 3 total trials).

(B) Viability of AGS and AGS 1q-loss cells treated with RX-3117. Mean ± SEM, data from representative trials are shown (n ≥ 3 total trials).

(C) A schematic displaying the generation of random aneuploid clones by transiently treating cells with an inhibitor of the spindle checkpoint kinase Mps1.

(D) SMASH karyotypes displaying the parental DLD1 cell line (top) and the DLD1 Trisomy 1 cell line (bottom) isolated used the approach displayed in (C).

(E) Viability of DLD1 and DLD1 Trisomy 1 cells treated with RX-3117. Mean ± SEM, data from representative trials are shown (n ≥ 3 total trials).

(F) Correlation between *UCK2* expression and sensitivity to RX-3117 (left) or 3-deazauridine (right) across the NCI-60 panel of cancer cell lines (*56*). Linear regression lines are plotted in red against the data.

Supplementary Figure 21

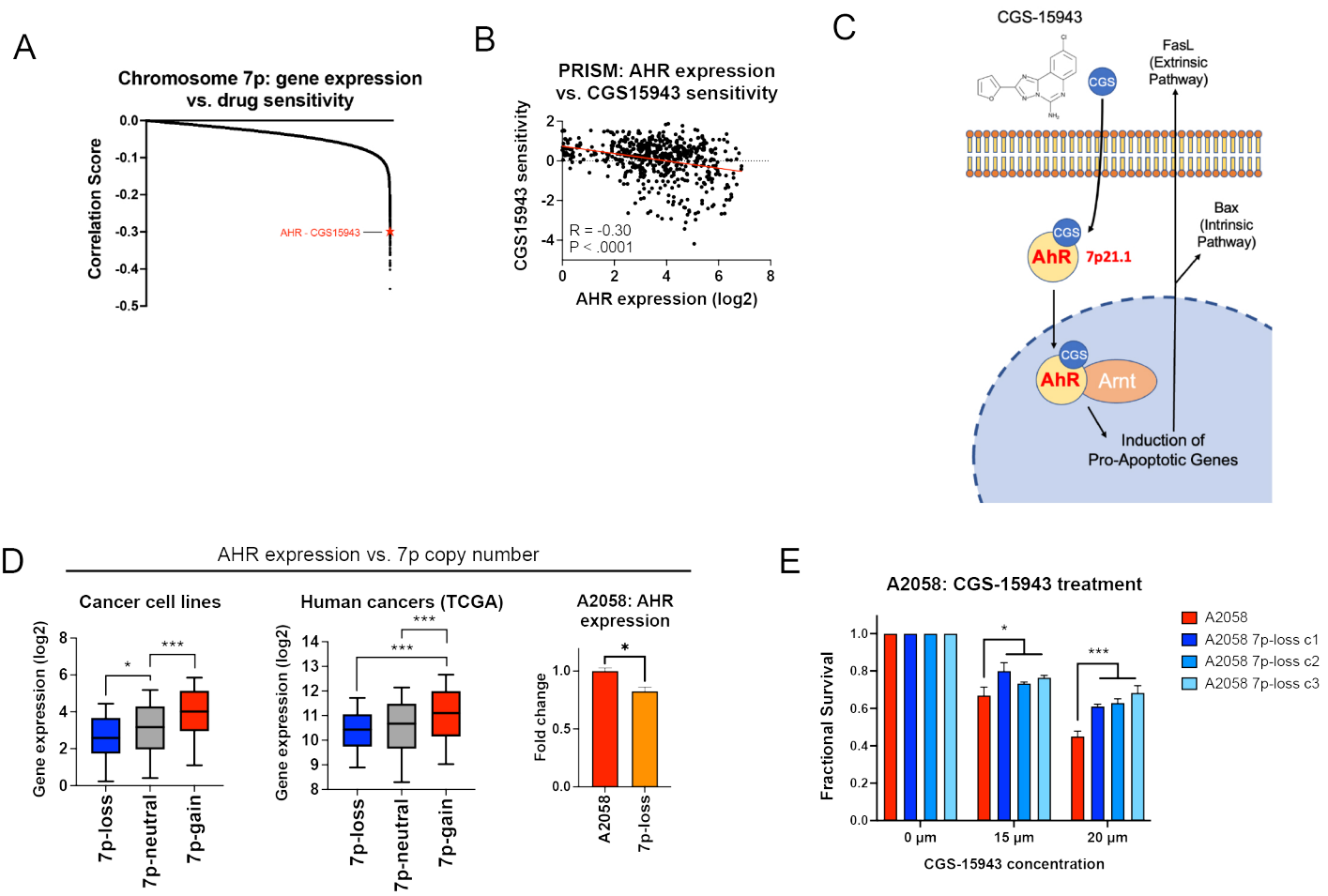

Figure S21. Identifying CGS-15943 as a compound that exhibits increased activity against cancer cells that are trisomic for chromosome 7p.

(A) A waterfall plot displaying all negative correlations between the expression of genes on chromosome 7p and drug sensitivity in the PRISM dataset (*57*). The AHR-CGS15493 dyad is indicated in red.

(B) A scatterplot displaying the correlation between *AHR* expression and CGS-15943 sensitivity. A linear regression line is plotted in red against the data.

(C) A schematic displaying how *AHR* expression is required for CGS-15943 sensitivity (*58*). CGS-15943 binds to AHR and Arnt and causes this complex to upregulate the expression of pro-apoptotic genes.

(D) Graphs displaying the relationship between chromosome 7p copy number and *AHR* expression. (Left and center): Boxplots displaying the expression of *AHR* from the cancer cell line encyclopedia (left) and TCGA (center), divided based on the copy number of chromosome 7p. (Right): A bar graph displaying the expression of *AHR* in wild-type A2058 cells and A2058 7p-disomic cells. The boxplots represent the 25th, 50th, and 75th percentiles of the indicated data, while the whiskers represent the 10th and 90th percentiles of the indicated data. The bar graph represents the mean ± SEM. Data were analyzed using unpaired t-tests.

(E) Cellular sensitivity of A2058 and A2058 7p-loss treated with different concentrations of CGS-15943.

*p < 0.05, ** p < 0.005, *** p < 0.0005

SUPPLEMENTAL TABLES

Table S1. Mutual exclusivity between chromosome gain events and mutations in cancer-associated genes.

Table S2. Association between chromosome copy number gains and cancer patient outcome.

Table S3. Aneuploidy-loss cell lines generated in this work.

Table S4. Sources of the cell lines used in this work.

Table S5. CRISPR and CRISPRi gRNA sequences used in this work.

Table S6. Overexpression plasmids used in this work.

Table S7. TaqMan copy number probes used in this work.

Table S8. TaqMan gene expression probes used in this work.

Table S9. Primers and oligonucleotides used in this work.

Table S10. Experimental data used to generate the figures in this work.